ISSN 0389-4010
UDC 533. 6. 011. 3
518. 61

TECHNICAL REPORT OF NATIONAL AEROSPACE LABORATORY

TR-1015T

Application of Jameson's Type Nonlinear Artificial Dissipation to the Two-Dimensional Navier-Stokes Computation

Nobuhiro KAWAI

February 1989

NATIONAL AEROSPACE LABORATORY

CHŌFU, TOKYO, JAPAN

Application of Jameson's Type Nonlinear Artificial Dissipation to the Two-Dimensional Navier-Stokes Computation*

Nobuhiro KAWAI**

ABSTRACT

In the present report, Jameson's nonlinear artificial dissipation model is studied so that the combination and modification of Jameson's type artificial dissipation model and Steger's one can be applied to Beam-Warming-Steger's implicit approximate factorization scheme for the Navier-Stokes equations.

Stability analysis is described for the algorithm where the combination of the explicit second-difference and fourth-difference artificial dissipation terms are added to the right-hand side and the implicit second-difference dissipation term is added to the left-hand side so that the system of equations can result in block tri-diagonal equations instead of penta-diagonal equations. And the details of the formulation of the artificial dissipation models, including the boundary approximation of the artificial dissipation, are described.

Numerical computations were made for transonic and low-speed flows, and the results show that the present formulation is appropriate. The effects of the artificial dissipation models are evaluated.

概　　要

Jameson の非線型人工散逸モデルを研究し，その結果，Jameson 型と Steger の人工散逸モデルの修正と組み合わせを，Navier-Stokes 方程式に対する Beam-Warming-Steger の Implicit Approximate Factorization 解法にうまく適合させることができた。

陽的2階および4階の人工散逸項の組み合わせを右辺に加え，陰的2階の散逸項を左辺に加える解法に対して，安定性解析を述べる。その結果，方程式系は5重対角方程式でなく，3重対角方程式に保つことができる。また，人工散逸の境界近似を含めて，人工散逸モデルの定式化を詳細に述べる。

数値計算を遷音速および低速流に対して行い，本定式化が妥当なことを示した。また，人工散逸モデルの影響を評価する。

1. INTRODUCTION

The implicit approximate factorization (IAF) scheme was devised by Beam and Warming[1] and established by Steger,[2] and it was a breakthrough of the computation of the Navier-Stokes equations. IAF scheme has been extended from two-dimensional flow problems to three-dimensional flow problems, and it is widely applied to various flow problems in many fields.

Various attempts have been done for the improvement of the IAF scheme in efficiency, accuracy or robustness. One of the most excellent improvements of the IAF scheme has been

* Received November 15, 1988
** Aircraft Aerodynamics Division

recently done by Pulliam.[3]. He has explained that many of modifications of the IAF scheme fall in the same category, namely, the use of a central difference approximation to the spatial derivatives and the addition of some form of artificial dissipation. And he has clarified how to apply Jameson's type nonlinear artificial dissipation to the IAF scheme. His formulation, however, results in the problem of solving penta-diagonal equations, which are inconvenient to handle.

The main purpose of the present report is to make the formulation where the inclusion of Jameson's type nonlinear artificial dissipation results in the problem of solving block tri-diagonal equations.

For this purpose, first, von Neumann stability analysis is made for the model equation which excludes a fourth-order dissipation term from the left-hand side. Next, so-obtained stability constraint is applied to the Navier-Stokes equations. Finally, the computations are done to verify the method of applying the stability constraint to the practical equations and to evaluate the merits and demerits of Jameson's type nonlinear artificial dissipation.

2. STABILITY ANALYSIS OF DISSIPATION OPERATORS FOR AN IMPLICIT ALGORITHM

Since it is very hard to analyze the stability of the Navier-Stokes equations, let us consider the linearilized one-dimensional scalar model equation as follows.

$$u_t + cu_x = \nu u_{xx} \tag{1}$$

Implicit difference form of Eq. (1) is

$$(1 + \lambda\delta - \mu\nabla\Delta)(u^{n+1} - u^n) = -\lambda\delta u^n + \mu\nabla\Delta u^n \tag{2}$$

where $\lambda = c\Delta t/\Delta x$, $\mu = \nu\Delta t/(\Delta x)^2$, and δ, ∇ and Δ are central, backward and forward difference operators, respectively. Adding artificial dissipation to Eq. (2), we get

$$(1 + \lambda\delta - \mu\nabla\Delta - \alpha_2\nabla\Delta + \alpha_4(\nabla\Delta)^2)(u^{n+1} - u^n) = -\lambda\delta u^n + \mu\nabla\Delta u^n + \beta_2\nabla\Delta u^n - \beta_4(\nabla\Delta)^2 u^n \tag{3}$$

where α_2, α_4, β_2 and β_4 are coefficients of the artificial dissipation terms. Pulliam[3] has analyzed the case where $\mu = 0$ and $\beta_2 = 0$ in Eq. (3). In the present report, we retain μ and β_2 but set $\alpha_4 = 0$. For simple description, we put

$$a = \alpha_2 + \mu \tag{4}$$

$$b = \beta_2 + \mu \tag{5}$$

Then Equation (3) becomes

$$(1 + \lambda\delta - a\nabla\Delta)(u_j^{n+1} - u_j^n) = -\lambda\delta u_j^n + b\nabla\Delta u_j^n - \beta_4(\nabla\Delta)^2 u_j^n \tag{6}$$

In order to apply the well-known von Neumann stability analysis, we let ω denote (the wave number) $\times$ (Δx) and i denote the imaginary unit, and we define the amplification factor as

$$g = u_j^{n+1}/u_j^n \tag{7}$$

We get the following relation from Eq. (6).

$$g = \frac{1+2(a-b)(1-\cos\omega)-4\beta_4(1-\cos\omega)^2}{1+2a(1-\cos\omega)+i\lambda\sin\omega} \tag{8}$$

Derivation of Eq. (8) from Eq. (6) is described in Appendix A.

To avoid complex discussion, we ignore the imaginary part of Eq. (8) by putting

$$\sin\omega = 0 \tag{9}$$

Then, Equation (8) changes to

$$g = \frac{1+2(a-b)(1-\cos\omega)-4\beta_4(1-\cos\omega)^2}{1+2a(1-\cos\omega)} \tag{10}$$

As described in detail in Appendix A, the absolute value of the right-hand side of Eq. (10) is greater than or equal to that of the right-hand side of Eq. (8). Therefore, the stability condition for Eq. (10) is satisfactory condition for the stability condition for Eq. (8).

We rewrite Eq. (10) as

$$g = 1 - 2b\,\frac{(1-\cos\omega)}{1+2a(1-\cos\omega)}$$

$$-4\beta_4 \frac{(1-\cos\omega)^2}{1+2a(1-\cos\omega)} \tag{11}$$

Since it is difficult to examine the magnitude of g in the form described by Eqs. (10) or (11), we rewrite Eq. (11) as follows.

$$g = 1 - 2by - 4\beta_4 z \tag{12}$$

where

$$y = \frac{x}{1+2ax} \tag{13}$$

and

$$z = \frac{x^2}{1+2ax} \tag{14}$$

with

$$x = 1 - \cos\omega \tag{15}$$

From Eq. (15), we find

$$0 \leqq x \leqq 2 \tag{16}$$

From Eq. (13), we find

$$\frac{dy}{dx} = \frac{1}{(1+2ax)^2} > 0 \tag{17}$$

for $a \geqq 0$ and $x \geqq 0$. From Eq. (14), we find

$$\frac{dz}{dx} = \frac{2x(1+ax)}{(1+2ax)^2} \geqq 0 \tag{18}$$

for $a \geqq 0$ and $x \geqq 0$. From the inequalities (17) and (18), we find that y and z are both monotonically increasing functions of x. Therefore, by the range of x, that is the inequality (16), and by Eqs. (13) and (14), we find the following ranges of y and z.

$$0 \leqq y \leqq \frac{2}{1+4a} \tag{19}$$

$$0 \leqq z \leqq \frac{4}{1+4a} \tag{20}$$

Note that y and z become minimum at the same time ($x = 0$), and that y and z become maximum at the same time ($x = 2$).

(Further note) $x = 0$ means $\cos\omega = 1$ and $x = 2$ means $\cos\omega = -1$. And they correspond to $\sin\omega = 0$, namely, to Eq. (9). At that moment, Equation (10) coincides with Eq. (8).

Assuming $b \geqq 0$ and $\beta_4 \geqq 0$, and substituting the ranges which are expressed by the inequalities (19) and (20) into Eq. (12), we get the following range of g.

$$1 - \frac{4b}{1+4a} - \frac{16\beta_4}{1+4a} \leqq g \leqq 1 \tag{21}$$

The von Neumann's stability criterion requires the following constraints.

$$-1 \leqq g \leqq 1 \tag{22}$$

One of the inequalities, $g \leqq 1$, of Eq. (22) has already been satisfied by Eq. (21). The other inequality, $-1 \leqq g$, of Eq. (22) requires the following inequality from Eq. (21).

$$-1 \leqq 1 - \frac{4b}{1+4a} - \frac{16\beta_4}{1+4a} \tag{23}$$

which can be rewritten as

$$\frac{1}{2}b + 2\beta_4 \leqq \frac{1}{4} + a \tag{24}$$

Substituting Eqs. (4) and (5) into the inequality (24), we get

$$\frac{1}{2}\beta_2 + 2\beta_4 \leqq \frac{1}{4} + \frac{1}{2}\mu + \alpha_2 \tag{25}$$

The inequality (25) is the von Neumann stability constraint of the model equation (1) in the implicit form written by Eq. (3) with $\alpha_4 = 0$. The coefficients, α_2, β_2 and β_4 are assumed constant.

However, if we apply Eq. (25) to practical computation, we have to consider that the nonlinear instability may occur since the Navier-Stokes equations are genuinely nonlinear, and that the coefficients of the artificial dissipation terms, α_2, β_2, β_4, may vary in space and time. Therefore, we should allow for the stability margin, and we set

$$\alpha_2 = \beta_2 + 2\beta_4 \tag{26}$$

Equation (26) satisfies the inequality (25), and is actually applied for the computation in the present report. The application of Eq. (26) to Jameson's type nonlinear artificial dissipation is described in Chapter 4 for the Navier-Stokes equations.

3. OUTLINE OF THE IMPLICIT APPROXIMATE FACTORIZATION SCHEME

The two-dimensional Navier-Stokes equations in general curvilinear coordinates where $\xi = \xi(x, y)$ and $\eta = \eta(x, y)$, can be written in a conservative form as

$$\partial_t \hat{Q} + \partial_\xi \hat{E} + \partial_\eta \hat{F} = \frac{1}{Re} (\partial_\xi \hat{R} + \partial_\eta \hat{S}) \quad (27)$$

where ∂_t, ∂_ξ and ∂_η are differential operators with respect to t, ξ and η respectively. In Eq. (27), the first term is an unsteady term, the second and third terms are convection terms, and the fourth and fifth terms are viscous terms. For the thin-layer approximation, we neglect the fourth term and the cross-derivative parts of the fifth terms.

If we define the Jacobian matrices

$$\hat{A} = \frac{\partial \hat{E}}{\partial \hat{Q}}, \quad \hat{B} = \frac{\partial \hat{F}}{\partial \hat{Q}}, \quad \hat{N} = \frac{\partial \hat{R}}{\partial \hat{Q}},$$

$$\hat{M} = \frac{\partial \hat{S}}{\partial \hat{Q}} \quad (28)$$

then the implicit approximate factorization scheme says that Equation (27) can be transformed to

$$\begin{aligned} &[I + \Delta t\, \partial_\xi \hat{A}^n - (\Delta t/Re)\, \partial_\xi \hat{N}^n - D_i|_\xi] \\ &\times [I + \Delta t\, \partial_\eta \hat{B}^n - (\Delta t/Re)\, \partial_\eta \hat{M}^n - D_i|_\eta] \\ &\times (\hat{Q}^{n+1} - \hat{Q}^n) \\ &= -\Delta t\, (\partial_\xi \hat{E}^n + \partial_\eta \hat{F}^n) + (\Delta t/Re) \\ &\times (\partial_\xi \hat{R}^n + \partial_\eta \hat{S}^n) + D_e|_\xi + D_e|_\eta \end{aligned} \quad (29)$$

where D_i and D_e denote artificial dissipation terms in the implicit and explicit parts respectively, and $|_\xi$ and $|_\eta$ indicate the directions of ξ and η respectively.

In the case of Steger's artificial dissipation, they can be written as

$$D_e|_\xi = -\epsilon_e \Delta t J^{-1} (\nabla_\xi \Delta_\xi)^2 J \hat{Q}^n \quad (30)$$

$$D_e|_\eta = -\epsilon_e \Delta t J^{-1} (\nabla_\eta \Delta_\eta)^2 J \hat{Q}^n \quad (31)$$

$$D_i|_\xi = \epsilon_i \Delta t J^{-1} \nabla_\xi \Delta_\xi J \quad (32)$$

$$D_i|_\eta = \epsilon_i \Delta t J^{-1} \nabla_\eta \Delta_\eta J \quad (33)$$

where Δ_ξ and ∇_ξ denote forward and backward difference operators in the ξ direction respectively, and Δ_η and ∇_η denote forward and backward difference operators in the η direction respectively. The coefficient ϵ_e is chosen to be $O(1)$ and $\epsilon_i = 2\epsilon_e$ in accordance with Eq. (26).

When we use Steger's artificial dissipation, the differential operators ∂_ξ of the convection terms, which are $\partial_\xi \hat{A}^n$ and $\partial_\xi \hat{E}^n$ in Eq. (29), are expressed by first-order-accurate upwind difference operator at a few points just before the shock wave in order to suppress shock capturing oscillation. And ∂_ξ is expressed by second-order-accurate central difference operator otherwise. The differential operator ∂_η is always expressed by second-order-accurate central difference operator, since we are interested in low speed or transonic flow in the present report.

The cross derivative parts of $\partial_\xi \hat{N}^n$ and $\partial_\eta \hat{M}^n$ are neglected so that the operators in each pair of the brackets, [ ], of Eq. (29) be in one direction.

Boundary conditions are given as follows. Along the far field boundary, the values of all the components of $\hat{Q}$ are fixed at the uniform-flow condition. Along the downstream boundary, the value of pressure is fixed at the uniform-flow condition, and the values of the other primitive variables are linearly extrapolated. Along the airfoil boundary, the velocity components are determined physically, namely, $u = v = 0$, and the numerical boundary conditions are determined by the continuity equation (for density) and the energy equation (for energy).

Baldwin and Lomax's algebraic turbulence model[4] is used. As for boundary-layer transition, the present code for computation has four options. The first is a "fully laminar" case where turbulence model is not used. This option is rarely used since we are interested in high Reynolds number flow. The second is a "fully turbulent" case where the boundary layer is turbulent everywhere. At the third option, Baldwin and Lomax's criterion[4] of transition is used. At the fourth option, Michel's criterion[5]

of transition is used.

4. PRACTICAL FORMULA OF ARTIFICIAL DISSIPATION FOR THE IMPLICIT SCHEME

Jameson's type nonlinear artificial dissipation is described below. And the result of the linear stability analysis described in Chapter 2 is applied to Jameson's type artificial dissipation in order to determine the form of $D_i|_\xi$ in Eq. (29).

Pulliam[3] has explained that first-order-accurate upwind difference is equivalent to a central difference plus second-difference artificial dissipation. Jameson's type nonlinear artificial dissipation consists of second-difference and fourth-difference artificial dissipation terms. Since second-difference artificial dissipation suppress shock capturing oscillation in place of first-order-accurate upwind differencing, we should use central differencing to the convection terms of Eq. (29) when we employ Jameson's type artificial dissipation. The detail explanation for the present paragraph is made for a simple case in Appendix B.

For preparation, we define

$$Q_{j,k} = J_{j,k}\,\hat{Q}_{j,k} \tag{34}$$

$$X_{j,k} = \nabla_\xi \Delta_\xi Q_{j,k} = Q_{j+1,k} - 2Q_{j,k} + Q_{j-1,k} \tag{35}$$

$$Y_{j,k} = \nabla_\eta \Delta_\eta Q_{j,k} = Q_{j,k+1} - 2Q_{j,k} + Q_{j,k-1} \tag{36}$$

Then, the explicit part of Jameson's type nonlinear artificial dissipation can be written as follows.

$$D_e|_\xi = \nabla_\xi (\sigma_{j+1,k} J^{-1}_{j+1,k} + \sigma_{j,k} J^{-1}_{j,k}) \times (\epsilon^{(2)}_{j,k} \Delta_\xi Q_{j,k} - \epsilon^{(4)}_{j,k} \Delta_\xi X_{j,k}) \tag{37}$$

with

$$\epsilon^{(2)}_{j,k} = \kappa_2 \Delta t \times \max(\Upsilon_{j+2,k}, \Upsilon_{j+1,k}, \Upsilon_{j,k}, \Upsilon_{j-1,k}) \tag{38}$$

and

$$\epsilon^{(4)}_{j,k} = \max(0, \kappa_4 \Delta t - \epsilon^{(2)}_{j,k}) \tag{39}$$

where typical values of the constants are $\kappa_2 = 1/4$ and $\kappa_4 = 1/100$.

Equation (38) is slightly modified from Pulliam's formula in order to keep symmetry with respect to the index j: Since the center of the index j for $\epsilon^{(2)}_{j,k}$ is $j + 1/2$, $\epsilon^{(2)}_{j,k}$ should have the components with indecies $(j+1, j)$ or $(j+2, j+1, j, j-1)$ or $(j+3, j+2, j+1, j, j-1, j-2)$ or ..... Therefore, another candidate for the definition of $\epsilon^{(2)}_{j,k}$ can be written as

$$\epsilon^{(2)}_{j,k} = \kappa_2 \Delta t \max(\Upsilon_{j+1,k}, \Upsilon_{j,k}) \tag{40}$$

The coefficient $\Upsilon_{j,k}$ at the point (j, k) is defined as

$$\Upsilon_{j,k} = \frac{|p_{j+1,k} - 2p_{j,k} + p_{j-1,k}|}{|p_{j+1,k} + 2p_{j,k} + p_{j-1,k}|} \tag{41}$$

where p denotes the pressure. The term of Eq. (37), $\sigma_{j,k}$, is the spectral radius of the matrix $\hat{A}$ and is defined as

$$\sigma_{j,k} = |U| + a\sqrt{\xi_x^2 + \xi_y^2} \tag{42}$$

where U is the ξ component of the contravariant velocity and a is the sonic speed. Equation (42) is modified from the Pulliam's formula, since he defined $\sigma_{j,k}$ as the sum of the spectral radii of $\hat{A}$ and $\hat{B}$.

To determine the implicit part of Jameson's type nonlinear dissipation, we utilize the result of Chapter 2. Comparing Eq. (37) with Eq. (3), we find the following correspondence.

$$\beta_2 = (\sigma_{j+1,k} J^{-1}_{j+1,k} + \sigma_{j,k} J^{-1}_{j,k})\,\epsilon^{(2)}_{j,k} \tag{43}$$

$$\beta_4 = (\sigma_{j+1,k} J^{-1}_{j+1,k} + \sigma_{j,k} J^{-1}_{j,k})\,\epsilon^{(4)}_{j,k} \tag{44}$$

By substituting Eqs. (43), (44) into Eq. (26), we get the following correspondence.

$$\alpha_2 = (\sigma_{j+1,k} J^{-1}_{j+1,k} + \sigma_{j,k} J^{-1}_{j,k}) \times (\epsilon^{(2)}_{j,k} + 2\,\epsilon^{(4)}_{j,k}) \tag{45}$$

Therefore, the implicit part of Jameson's type nonlinear artificial dissipation can be written as

$$D_i|_\xi = \nabla_\xi (\sigma_{j+1,k} J^{-1}_{j+1,k} + \sigma_{j,k} J^{-1}_{j,k}) \times \epsilon^{(i)}_{j,k} \Delta_\xi J_{j,k} \tag{46}$$

with

$$\epsilon_{j,k}^{(i)} = \epsilon_{j,k}^{(2)} + 2\,\epsilon_{j,k}^{(4)} \tag{47}$$

Equations (46) and (47) are the main result of the present Chapter. Strictly speaking, the above derivation does not assure the stability, since the discussion of Chapter 2 is based on linear theory with constant coefficients while the right-hand sides of Eqs. (43), (44) and (45) are variable coefficients. However, this kind of generalization is adequate for many practical problems.[6] We have made computation to verify Eqs. (46) and (47), and the stability is achieved for the Navier-Stokes equations as discussed in Chapter 6, 7 and 8.

The above discussion deals with the artificial dissipation in the ξ direction. So let us discuss Jameson's type nonlinear artificial dissipation in the η direction. The development of equations about the η-direction dissipation is the same as the above discussion, and only the resulting equations will be described below.

The explicit part of Jameson's type nonlinear artificial dissipation can be written as

$$D_e|_\eta = \nabla_\eta (\tilde{\sigma}_{j,k+1} J_{j,k+1}^{-1} + \tilde{\sigma}_{j,k} J_{j,k}^{-1}) \times (\tilde{\epsilon}_{j,k}^{(2)} \Delta_\eta Q_{j,k} - \tilde{\epsilon}_{j,k}^{(4)} \Delta_\eta Y_{j,k}) \tag{48}$$

with

$$\tilde{\epsilon}_{j,k}^{(2)} = \kappa_2 \Delta t \times \max(\tilde{\Upsilon}_{j,k+2}, \tilde{\Upsilon}_{j,k+1}, \tilde{\Upsilon}_{j,k}, \tilde{\Upsilon}_{j,k-1}) \tag{49}$$

and

$$\tilde{\epsilon}_{j,k}^{(4)} = \max(0, \kappa_4 \Delta t - \tilde{\epsilon}_{j,k}^{(2)}) \tag{50}$$

Another candidate for $\tilde{\epsilon}_{j,k}^{(2)}$ can be written as

$$\tilde{\epsilon}_{j,k}^{(2)} = \kappa_2 \Delta t \max(\tilde{\Upsilon}_{j,k+1}, \tilde{\Upsilon}_{j,k}) \tag{51}$$

The coefficient $\tilde{\Upsilon}_{j,k}$ is defined as

$$\tilde{\Upsilon}_{j,k} = \frac{|p_{j,k+1} - 2p_{j,k} + p_{j,k-1}|}{|p_{j,k+1} + 2p_{j,k} + p_{j,k-1}|} \tag{52}$$

$\tilde{\sigma}_{j,k}$ is the spectral radius of the matrix $\hat{B}$ and is defined as

$$\tilde{\sigma}_{j,k} = |V| + a\sqrt{\eta_x^2 + \eta_y^2} \tag{53}$$

where V is the η component of the contravariant velociy. The implicit part of Jameson's type nonlinear artificial dissipation in η direction can be written as

$$D_i|_\eta = \nabla_\eta (\tilde{\sigma}_{j,k+1} J_{j,k+1}^{-1} + \tilde{\sigma}_{j,k} J_{j,k}^{-1}) \times \tilde{\epsilon}_{j,k}^{(i)} \Delta_\eta J_{j,k} \tag{54}$$

with

$$\tilde{\epsilon}_{j,k}^{(i)} = \tilde{\epsilon}_{j,k}^{(2)} + 2\,\tilde{\epsilon}_{j,k}^{(4)} \tag{55}$$

When we use Eqs. (48) through (55) in computing the Navier-Stokes equations, there is no problem of stability or convergence, but there is a problem of accuracy. Since Equation (48) includes second-difference artificial dissipation and this artificial dissipation behaves like actual viscosity, the computed viscosity is actual viscosity plus the spurious viscosity caused by the second-difference artificial dissipation. Maybe this detrimental effect of the artificial dissipation can be improved by factoring M^2 to the right-hand side of Eq. (48), where M denotes local Mach number. But the author has not tried it yet.

Instead of using Jameson's type nonlinear artificial dissipation in η direction, we use Steger's type artificial dissipation in η direction with slight modification. By using the definition (36), Equation (31) becomes

$$D_e|_\eta = -f\epsilon_e \Delta t J_{j,k}^{-1} \nabla_\eta \Delta_\eta Y_{j,k} \tag{56}$$

where f is a modification factor and is usually taken as $f = 1$. To reduce the effect of artificial dissipation as small as possible, we define the modification factor as

$$f = \frac{u^2 + v^2}{u_e^2 + v_e^2} \tag{57}$$

where u and v are velocity components in Cartesian coordinates, and the subscript e indicates the edge of the boundary layer. Since it costs considerable computation time to seek the edge of the boundary layer, we employ Eq. (57) only when we use Michel's criterion of boundary-layer transition. Because we seek the

boundary-layer edge when we use Michel's criterion. Outside the boundary-layer edge, f is always set to $f = 1$.

5. BOUNDARY APPROXIMATION FOR ARTIFICIAL DISSIPATION

Since fourth-difference artificial dissipation consists of five-point values of $Q_{j,k}$, it encounters difficulty at the points adjacent to the boundaries. Because one of $Q_{j,k}$'s goes out of the domain of interest. Therefore, we have to approximate fourth-difference artificial dissipation at the points adjacent to the boundaries. And the approximation have to be stable.

Seeing Eqs. (37) and (48), we find that fourth-difference artificial dissipation requires the boundary values of $X_{j,k}$ and $Y_{j,k}$. In other words, the second difference of $X_{j,k}$ or $Y_{j,k}$ at the point adjacent to the boundary requires the boundary value of $X_{j,k}$ or $Y_{j,k}$. Let us explain it concretely. Letting the indices take the values as $j = 1$, $j = jmax$, $k = 1$, $k = kmax$ at the boundaries, we find by definition, Eq. (35), that

$$X_{1,k} = Q_{2,k} - 2Q_{1,k} + Q_{0,k} \tag{58}$$

But $Q_{0,k}$ is a physical quantity at a fictitious point ($j = 0$), and so $X_{1,k}$ cannot be rigorously determined.

Pulliam[3] asserts, in our notation, that the formula

$$X_{1,k} = 0 \tag{59}$$

gives the least detrimental effect on the accuracy for practical computations. Equation (59) means that $Q_{0,k}$ and $Q_{2,k}$ are symmetrical with regard to the point $Q_{1,k}$. On the other hand, the reflective condition can be written as

$$Q_{0,k} = Q_{2,k} \tag{60}$$

or

$$X_{1,k} = 2(Q_{2,k} - Q_{1,k}) \tag{61}$$

There are many possible approximations besides Eqs. (59) and (61). For example, $X_{1,k} = X_{2,k}$ and $X_{1,k} = -X_{2,k}$ are the candidates of the boundary approximation for the fourth-difference artificial dissipation. In the present report, we employ the following boundary approximation.

$$Q_{0,k} = Q_{1,k} \tag{62}$$

or

$$X_{1,k} = Q_{2,k} - Q_{1,k} \tag{63}$$

Equation (63) is the intermediate approximation between Eqs. (59) and (61), and seems to give the least detrimental effect on the accuracy. Similarly, we employ the following approximations.

$$X_{jmax,k} = Q_{jmax-1,k} - Q_{jmax,k} \tag{64}$$

$$Y_{j,1} = Q_{j,2} - Q_{j,1} \tag{65}$$

$$Y_{j,kmax} = Q_{j,kmax-1} - Q_{j,kmax} \tag{66}$$

To examine the stability nature of the boundary approximations described by Eqs. (63), (64), (65) and (66) for the artificial dissipation, we consider the model equation

$$du_j/dt = -\nabla\Delta X_j \tag{67}$$

$$X_j = \nabla\Delta u_j \tag{68}$$

for $j = 2$ to $n-1$. Here $j = 1$ and $j = n$ indicate the boundary points, and Δ and ∇ are forward and backward difference operators respectively. Boundary approximation of X_j corresponding to Eqs. (63), (64), (65) and (66) can be written as

$$X_1 = u_2 - u_1 \tag{69}$$

$$X_n = u_{n-1} - u_n \tag{70}$$

Therefore

$$\begin{aligned}\nabla\Delta X_2 &= (u_4 - 2u_3 + u_2) - 2(u_3 - 2u_2 + u_1) \\ &\quad + (u_2 - u_1) \\ &= -3u_1 + 6u_2 - 4u_3 + u_4\end{aligned} \tag{71}$$

and

$$\begin{aligned}\nabla\Delta X_{n-1} &= (u_{n-1} - 2u_{n-2} + u_{n-3}) \\ &\quad - 2(u_n - 2u_{n-1} + u_{n-2}) \\ &\quad + (u_{n-1} - u_n) \\ &= -3u_n + 6u_{n-1} - 4u_{n-2} + u_{n-3}\end{aligned} \tag{72}$$

As a matter of course

$$\nabla\Delta X_j = u_{j-2} - 4u_{j-1} + 6u_j - 4u_{j+1} + u_{j+2} \tag{73}$$

for $j = 3$ to $n-2$. We neglect u_1 and u_n as

$$u_1 = u_n = 0 \tag{74}$$

because u_1 and u_n do not change their values temporarily when we solve model equation (67) with Eq. (68), that is, the perturbations of the boundary values, u_1 and u_n, are temporarily zero. Then substituting Eqs. (71), (72), (73) and (74) into Eq. (67), we get a vector-matrix form as

$$du/dt = \boldsymbol{A}\boldsymbol{u} \tag{75}$$

where

$$\boldsymbol{u} = \begin{bmatrix} u_2 \\ u_3 \\ \vdots \\ u_{n-1} \end{bmatrix} \tag{76}$$

and

$$\boldsymbol{A} = -\begin{bmatrix} 6 & -4 & 1 & & & & & \mathrm{O} \\ -4 & 6 & -4 & 1 & & & & \\ 1 & -4 & 6 & -4 & 1 & & & \\ & 1 & -4 & 6 & -4 & 1 & & \\ & & \cdots & \cdots & \cdots & \cdots & \cdots & \\ & & & 1 & -4 & 6 & -4 & 1 \\ & & & & 1 & -4 & 6 & -4 \\ \mathrm{O} & & & & & 1 & -4 & 6 \end{bmatrix} \tag{77}$$

We will discuss the stability of Eq. (75) in the following paragraphs.

In this paragraph, we show the well-known fact that if we can diagonalize A and if the real part of any of the eigenvalues of A is negative, then the solution of Eq. (75) tends to zero vector. It is well known (See Appendix C) that

$$\boldsymbol{u} = \exp(\boldsymbol{A}t) \tag{78}$$

is a particular solution of Eq. (75). If we assume that we are able to diagonalize A as

$$\boldsymbol{S}^{-1}\boldsymbol{A}\boldsymbol{S} = \Lambda \tag{79}$$

then Eq. (78) becomes (See Appendix C)

$$\boldsymbol{u} = \exp(\boldsymbol{A}t) = \boldsymbol{S}\exp(\Lambda t)\,\boldsymbol{S}^{-1} \tag{80}$$

Letting $\lambda_2, \lambda_3, \lambda_4, \ldots, \lambda_{n-1}$ be the eigenvalues of matrix A, we can express $\exp(\Lambda t)$ by the following formula (See Appendix C).

$$\exp(\Lambda t) = \begin{bmatrix} \exp(\lambda_2 t) & & & \mathrm{O} \\ & \exp(\lambda_3 t) & & \\ & & \ddots & \\ \mathrm{O} & & & \exp(\lambda_{n-1} t) \end{bmatrix} \tag{81}$$

Substituting Eq. (81) into Eq. (80), we obtain

$$\boldsymbol{u} = \boldsymbol{S}\begin{bmatrix} \exp(\lambda_2 t) & & & \mathrm{O} \\ & \exp(\lambda_3 t) & & \\ & & \ddots & \\ \mathrm{O} & & & \exp(\lambda_{n-1} t) \end{bmatrix}\boldsymbol{S}^{-1} \tag{82}$$

as a particular solution of Eq. (75). Therefore, if any of the real part of the eigenvalues, $\lambda_2, \lambda_3, \ldots, \lambda_{n-1}$, of the matrix A is negative, u tends to zero vector as t increases, since S is a constant matrix.

It is almost impossible to analytically find eigenvalues of the matrix A. Instead, we form the matrix A for a specified value of n (we take the values as $n = 10, 22, 62, 72, 82$ for example), and use computer software to compute the eigenvalues numerically. In any case the author has tried, the numerically computed eigenvalues of matrix A are real, negative and distinct. Therefore, the assumption made on Eq. (78) hold true, and the vector u is numerically shown to tend to zero vector. That is to say, the model equation (67) with Eq. (68) is stable when we use the boundary approximation described by Eqs. (69) and (70).

The above discussion is not rigorous for a few reasons. The assumption described by Eq. (74) is not rigorous especially when it interacts with boundary condition. The model equation (67) with (68) does not include convection term nor viscous term. The practical equations are

nonlinear, though the above discussion is linear. However, the above discussion is useful as a guideline. That is, the application of the boundary approximation (69) and (70), namely, Eqs. (63), (64), (65) and (66), is used successfully for practical computations, and the solution is stable with these boundary approximations.

6. RESULT FOR NACA 0012 AIRFOIL

The main part of the present method is the formulation of the implicit part of Jameson's type nonlinear artificial dissipation. And it is expressed by Eqs. (46) and (47). We also use Steger's artificial dissipation described by Eqs. (30) and (32) for comparison. In the η direction, however, we use the slightly modified Steger's artificial dissipation described by Eqs. (33), (56) and (57) except for the computation shown in Fig. 6.

To verify the present method and to compare the present artificial dissipation (Jameson's type) with Steger's artificial dissipation, the computation was done for the transonic flow around an NACA 0012 airfoil. The flow condition is chosen as; free stream Mach numbers of 0.75 and 0.8, an attack angle of 2 degree, and a Reynolds number of 20 million. The grid is composed of 241 points in the ξ direction and 65 points in the η direction. The minimum grid space in the η direction is 1.0×10^{-5} when the chord length is set to be unity. The grid near the airfoil (20 points in the η direction) is generated algebraically so that the grid near the airfoil be exactly orthogonal to the surface of the airfoil. This orthogonality improves the numerical accuracy. The rest of the grid is generated by the method of elliptic equations.

First let us discuss the case of $M_\infty = 0.75$. Figures 1, 2 and 3 are the results computed by the present method. That is, we use Eqs. (37), (38), (39), (41), (42), (46) and (47). The coefficients of the artificial dissipation terms are set as; $\kappa_2 = 0.25$, $\kappa_4 = 0.01$, $\epsilon_e = 2.0$ and $\epsilon_i = 4.0$ for Figs. 1 and 2, and $\kappa_2 = 0.35$, $\kappa_4 = 0.014$, $\epsilon_e = 2.0$ and $\epsilon_i = 4.0$ for Fig. 3. Figures 4 and 5 are the results computed by using Steger's artificial dissipation in both ξ- and η-directions. The coefficients of the artificial dissipation terms are set as; $\epsilon_e = 4.0$ and $\epsilon_i = 8.0$ for Figs. 4 and 5. (a) of Figures 1 through 5 indicates the pressure coefficient distribution, and (b) of these figures indicates the skin friction coefficient distribution. Figures 1 and 4 are the results computed by using Michel's criterion of boundary-layer transition. Figures 2 and 5 are the results computed by the condition of fully-turbulent boundary layer, and Figure 3 is the result computed by using Baldwin-Lomax's criterion of boundary-layer transition. When Steger's artificial dissipation was used with Baldwin-Lomax's criterion of boundary-layer transition, the numerical solution burst.

Figures 1, 2 and 3 show that the computation with the present method for the artificial dissipation is stable and reliable. On one hand, Figures 1a, 2a and 3a show that there is no spurious overshoot of the pressure coefficient distribution just before the shock wave when we use Jameson's type nonlinear artificial dissipation with the present method. On the other hand, Figures 4a and 5a show that there is a spurious overshoot of the pressure coefficient distribution just before the shock wave when we use Steger's artificial dissipation in both ξ- and η-direction. We also find that Jameson's type artificial dissipation (Figs. 1a, 2a, 3a) gives sharper shock wave than Steger's artificial dissipation (Figs. 4a, 5a). The undershoot of the pressure coefficient distribution just after the shock wave appears in Figs. 1a and 4a, since the boundary-layer thickness is thin when we use Michel's criterion of boundary-layer transition.

In computing the result of Fig. 6, we use Jameson's type artificial dissipation in both ξ- and η-directions. That is, we use Eqs. (48) through (55) (except for Eq. (51)) to examine the effect of Jameson's type artificial dissipation in the η direction. Although we cannot find

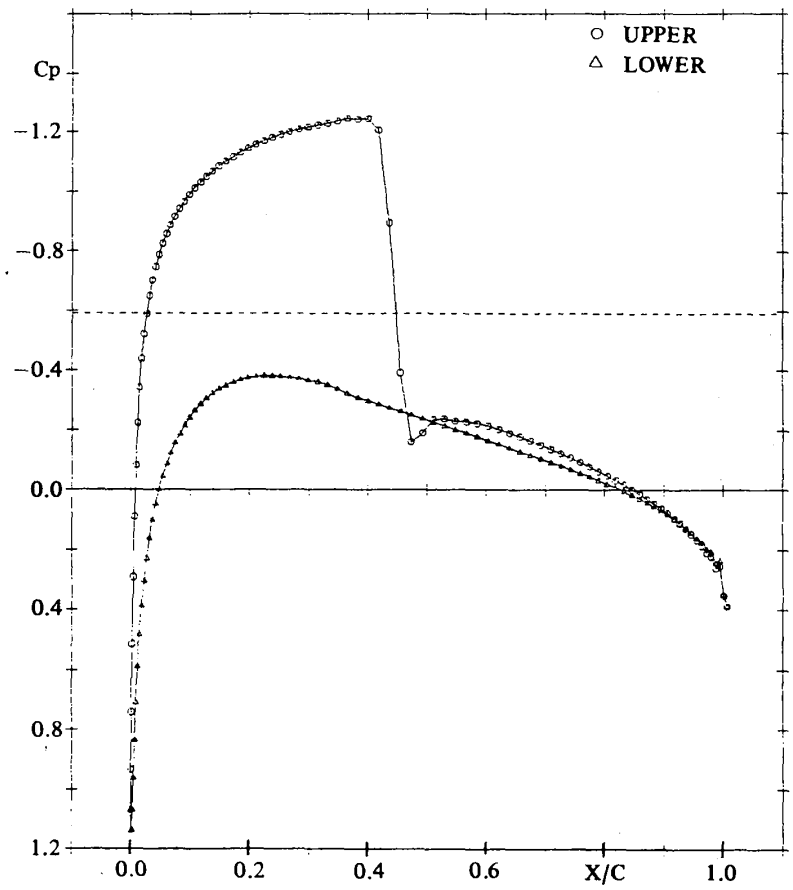

(a) Pressure coefficient distribution.

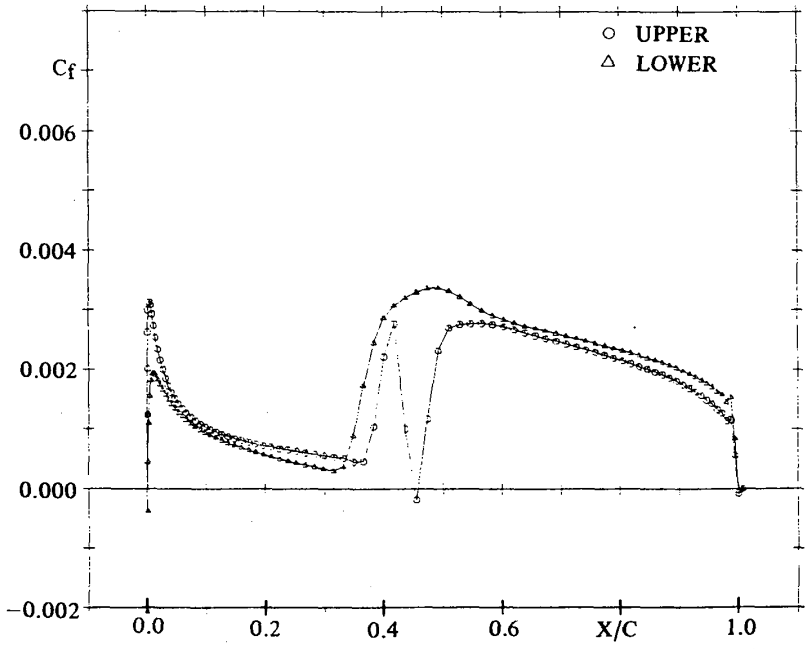

(b) Skin friction coefficient distribution.

Fig. 1 Result for NACA 0012, $M_\infty = 0.75$, $\alpha = 2^\circ$, $Re = 2 \times 10^7$.
Present artificial dissipation. Michel's criterion of transition.
$\kappa_2 = 0.25$, $\kappa_4 = 0.01$, $\epsilon_e = 2.0$, $\epsilon_i = 4.0$,
$C_L = 0.37281$, $C_D = 0.01434$, $C_M = 0.00097$.

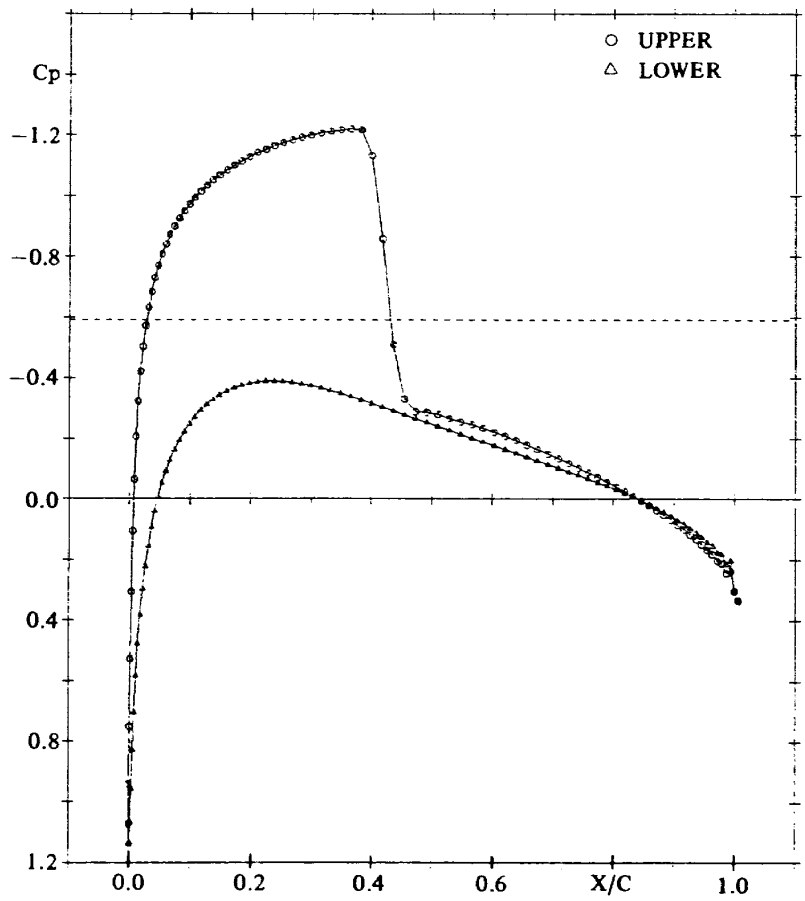

(a) Pressure coefficient distribution.

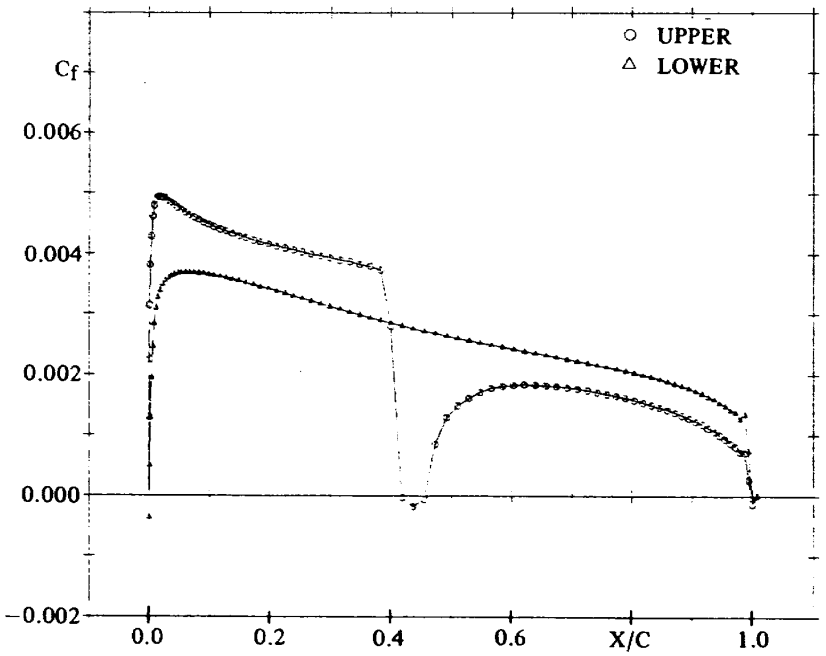

(b) Skin friction coefficient distribution.

Fig. 2 Result for NACA 0012, $M_\infty = 0.75$, $\alpha = 2^\circ$, $Re = 2 \times 10^7$.
Present artificial dissipation. Fully turbulent.
$\kappa_2 = 0.25$, $\kappa_4 = 0.01$, $\epsilon_e = 2.0$, $\epsilon_i = 4.0$,
$C_L = 0.34333$, $C_D = 0.01603$, $C_M = 0.00605$.

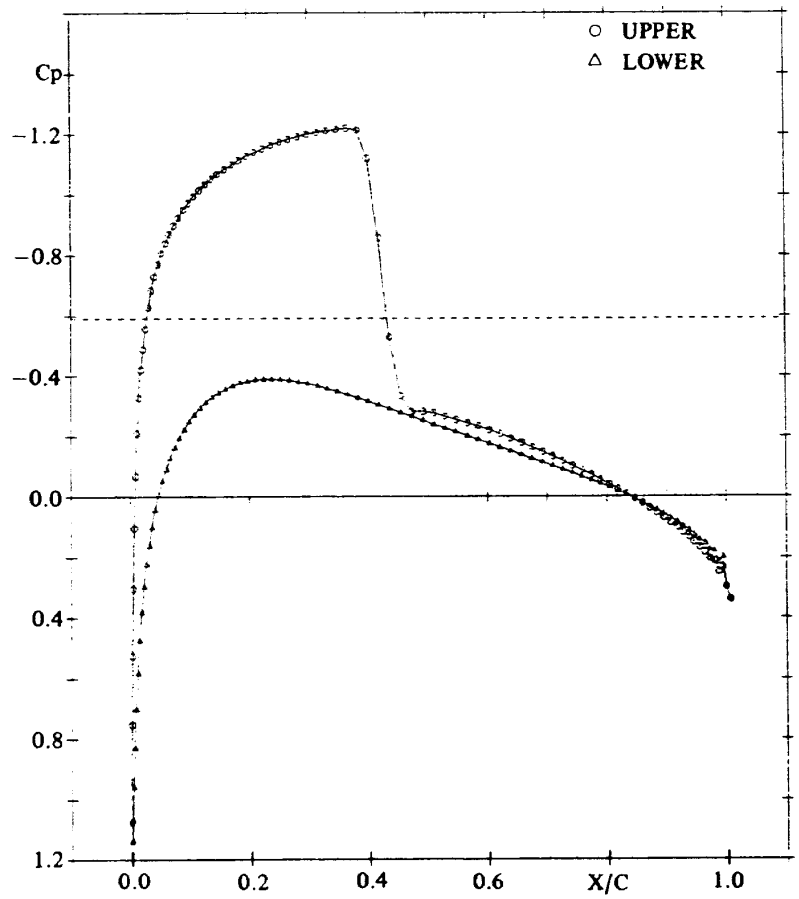

(a) Pressure coefficient distribution.

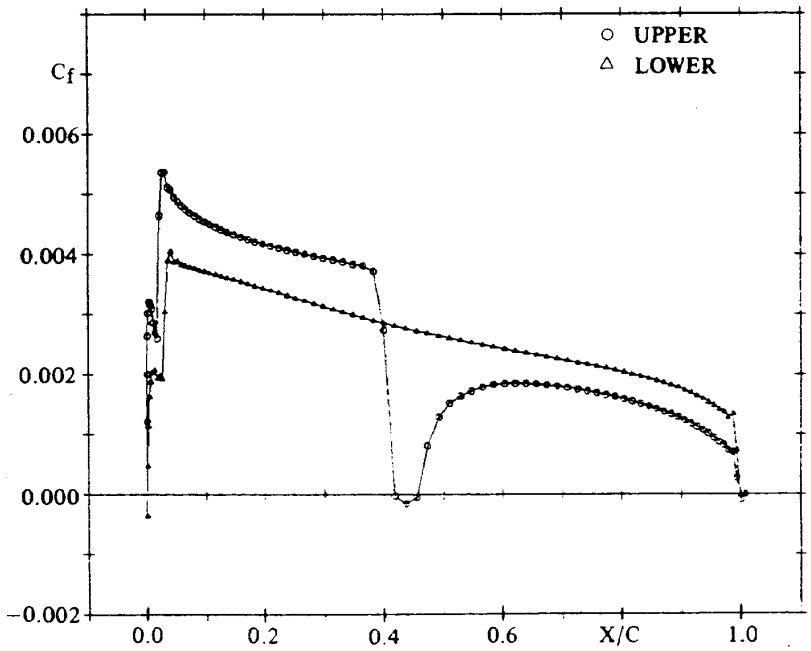

(b) Skin friction coefficient distribution.

Fig. 3 Result for NACA 0012, $M_\infty = 0.75$, $\alpha = 2^\circ$, $Re = 2 \times 10^7$.
Present artificial dissipation. Baldwin-Lomax's criterion of transition.
$\kappa_2 = 0.35$, $\kappa_4 = 0.014$, $\epsilon_e = 2.0$, $\epsilon_i = 4.0$,
$C_L = 0.34296$, $C_D = 0.01602$, $C_M = 0.00616$.

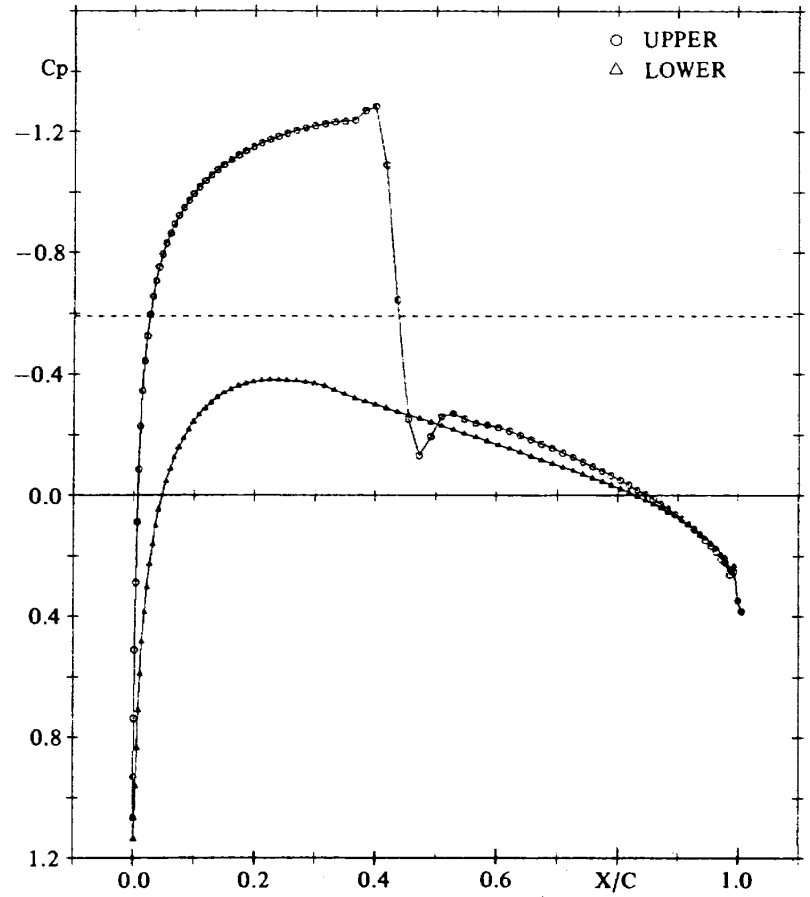

(a) Pressure coefficient distribution.

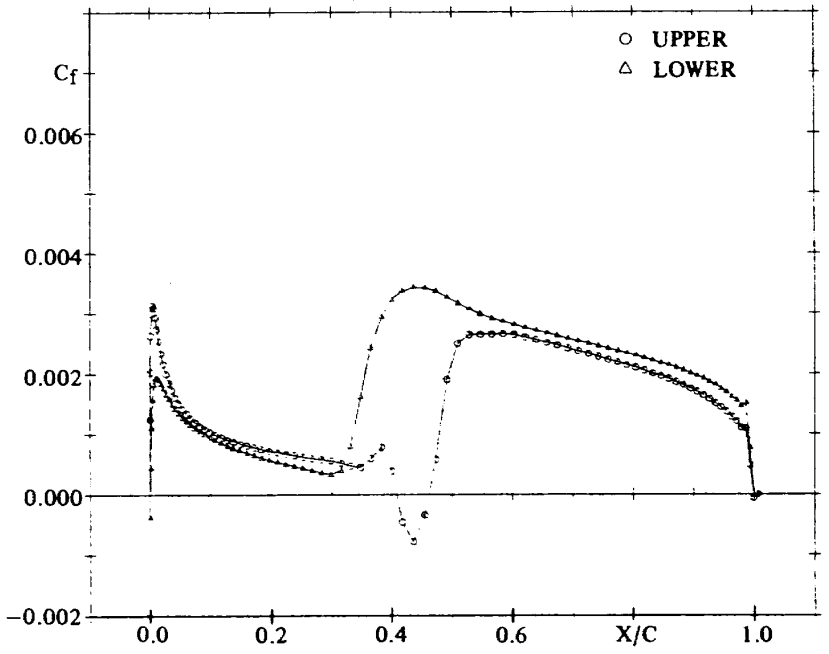

(b) Skin friction coefficient distribution.

Fig. 4 Result for NACA 0012, $M_\infty = 0.75$, $\alpha = 2°$, $Re = 2 \times 10^7$.
Steger's artificial dissipation. Michel's criterion of transition.
$\epsilon_e = 4.0$, $\epsilon_i = 8.0$.
$C_L = 0.36688$, $C_D = 0.01366$, $C_M = 0.00223$.

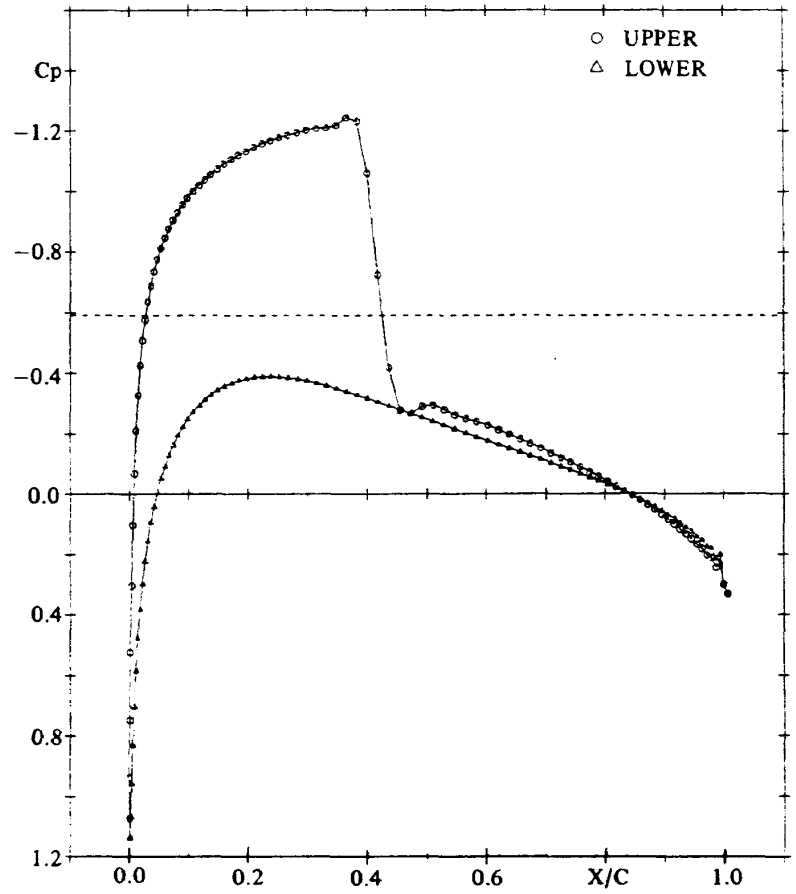

(a) Pressure coefficient distribution.

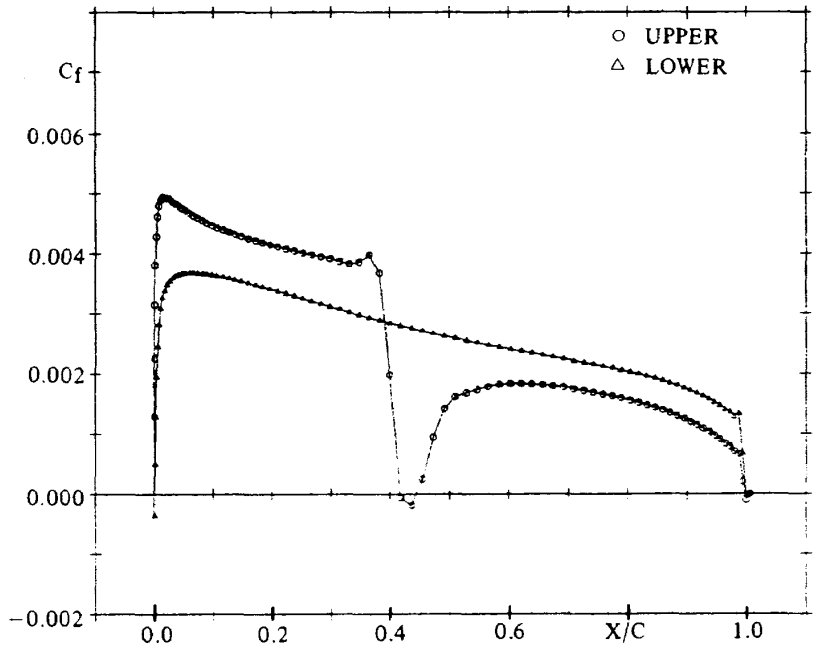

(b) Skin friction coefficient distribution.

Fig. 5 Result for NACA 0012, $M_\infty = 0.75$, $\alpha = 2^\circ$, $Re = 2 \times 10^7$.
Steger's artificial dissipation. Fully turbulent.
$\epsilon_e = 4.0$, $\epsilon_i = 8.0$,
$C_L = 0.33973$, $C_D = 0.01556$, $C_M = 0.00695$.

much difference in the pressure coefficient distribution when we compare Fig. 6a with Fig. 1a, we find significant difference in the distributions of the surface skin friction when we compare Fig. 6b with Fig. 1b. Jameson's type artificial dissipation in the η direction described by Eq. (55) has second-order difference, and it behaves like viscous term. The spurious viscosity which comes from the second-order difference of Jameson's type artificial dissipation, becomes noticeable and turbulent region of the boundary layer becomes fictitiously large as seen in Fig. 6b. That is why we do not employ Jameson's type nonlinear artificial dissipation in the η direction except for the case shown by Fig. 6, but employ the slightly modified Steger's artificial dissipation in the η direction.

This detrimental effect of Jameson's type nonlinear artifial dissipation in the η direction is clarified by using Michel's criterion of boundary-layer transition. When we use Baldwin-Lomax's criterion of transition, the transition point is very near the leading edge as seen in Fig. 3(b), and if we use Jameson's type artificial dissipation in the η direction, the forward movement of the transition point is not clear. Since the eddy viscosity of the turbulent boundary layer is large by nature, the increase of viscosity which is caused by the Jameson's type nonlinear artificial dissipation in the η direction is not clear.

Next let us discuss the case of $M_\infty = 0.8$ to show that the present method is applicable to the flow with stronger shock wave. Figures 7, 8 and 9 are the results computed by the present method, where Jameson's type nonlinear artificial dissipation is used in the ξ direction and the slightly modified Steger's artificial dissipation is used in the η direction. Figures 10 and 11 are the results computed by using Steger's artificial dissipation in both ξ- and η-directions. (a) of Figs. 7 through 11 indicates the pressure coefficient distribution. (b) of these figures indicates the skin friction coefficient distribution. Figures 7 and 10 are the results computed by using Michel's criterion of boundary-layer transition, Figures 8 and 11 are the results computed by the condition of fully-turbulent boundary layer, and Figure 9 is results computed by using Baldwin-Lomax's criterion of boundary-layer transition. Here again, the numerical solution burst when Steger's artificial dissipation was used with Baldwin-Lomax' criterion of transition. So we have the impression that Jameson's type nonlinear artificial dissipation gives robuster numerical solution than Steger's one.

Since there is no overshoot just before the shock wave in the pressure coefficient distributions of Fig. 7a, 8a and 9a, we find that Jameson's type artificial dissipation is suitable to capture shock wave. There is no undershoot just after the shock wave in the pressure coefficient distributions of these figures, either. Because there is a separation bubble at the foot of shock wave in each of these results, and the shock wave interacts with the separation bubble. Figures 7b, 8b and 9b show that each of the upper distributions of the skin friction coefficient has the region where the skin friction coefficient is negative (about 67% chord length). This part indicates a separation bubble, which is induced by a strong shock wave. There is no overshoot just before the shock wave in the pressure coefficient distribution of Fig. 10a, but there is a small overshoot just before the shock wave in the pressure coefficient distribution of Fig. 11a. These facts imply that Steger's artificial dissipation sometimes brings about a spurious overshoot just before shock wave. The undershoot of the pressure coefficient distribution just behind the shock wave does not appear in any of these figures, because there is a separation bubble as seen in Figs. 10b and 11b, and the shock wave interacts with the separation bubble.

The results of the present Chapter show that the computation by the present method for Jameson's type nonlinear artificial dissipation is successful and is adequate to capturing shock wave. But if we employ Jameson's type non-

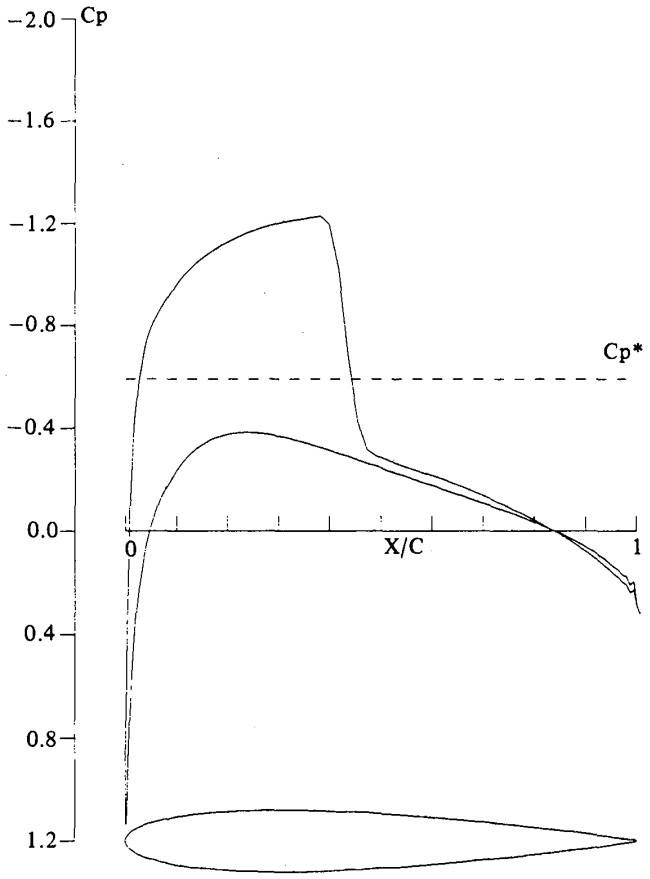

(a) Pressure coefficient distribution.

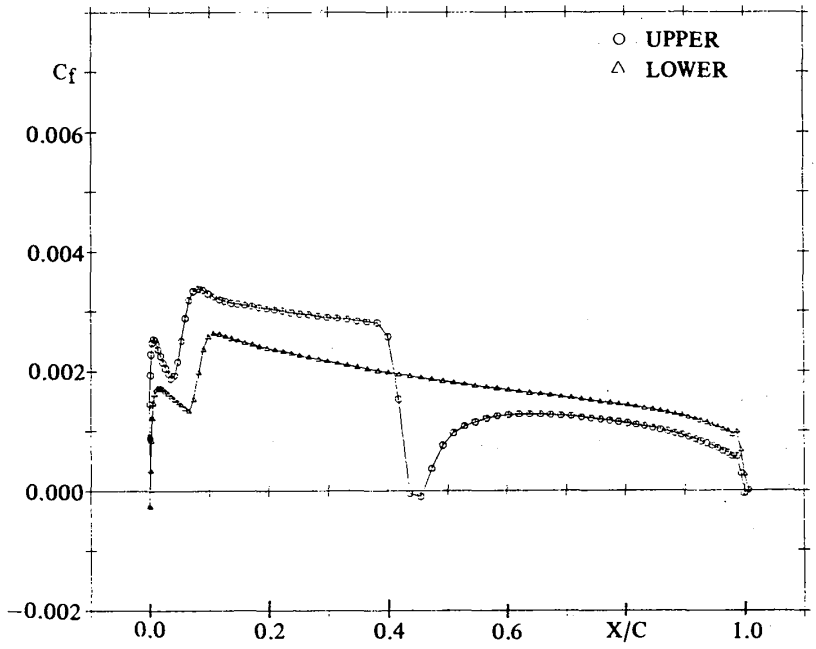

(b) Skin friction coefficient distribution.

Fig. 6 Result for NACA 0012, $M_\infty = 0.75$, $\alpha = 2^\circ$, $Re = 2 \times 10^7$.
Jameson's type nonlinear artificial dissipation is used in both ξ- and η-directions. Michel's criterion of transition.
$\kappa_2 = 0.25$, $\kappa_4 = 0.01$,
$C_L = 0.35278$, $C_D = 0.01558$, $C_M = 0.00528$.

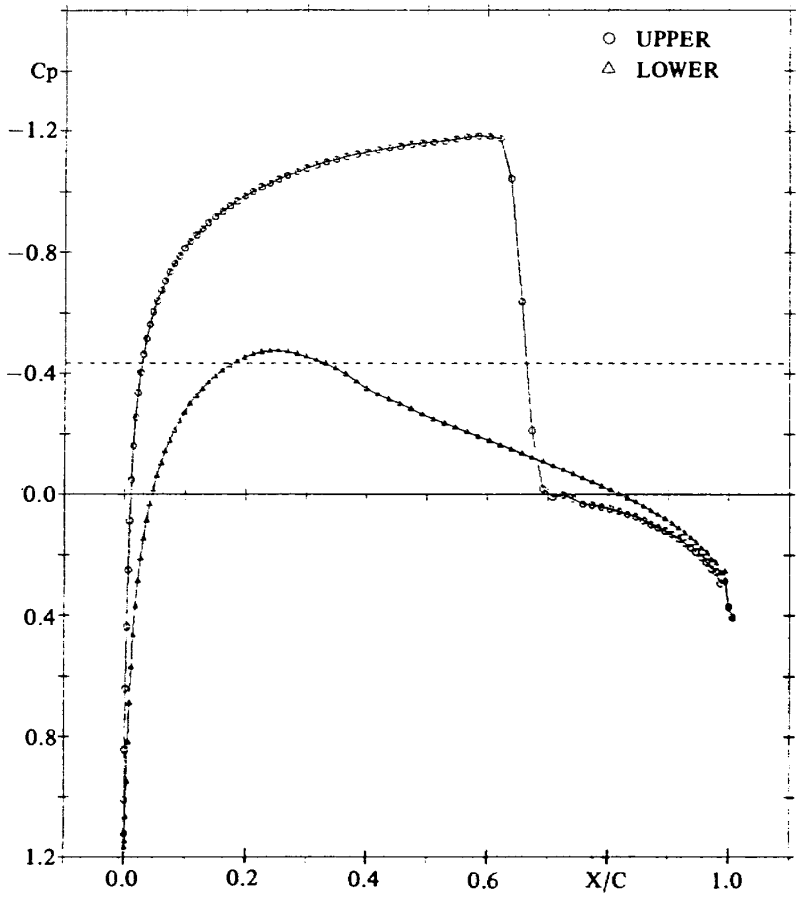

(a) Pressure coefficient distribution.

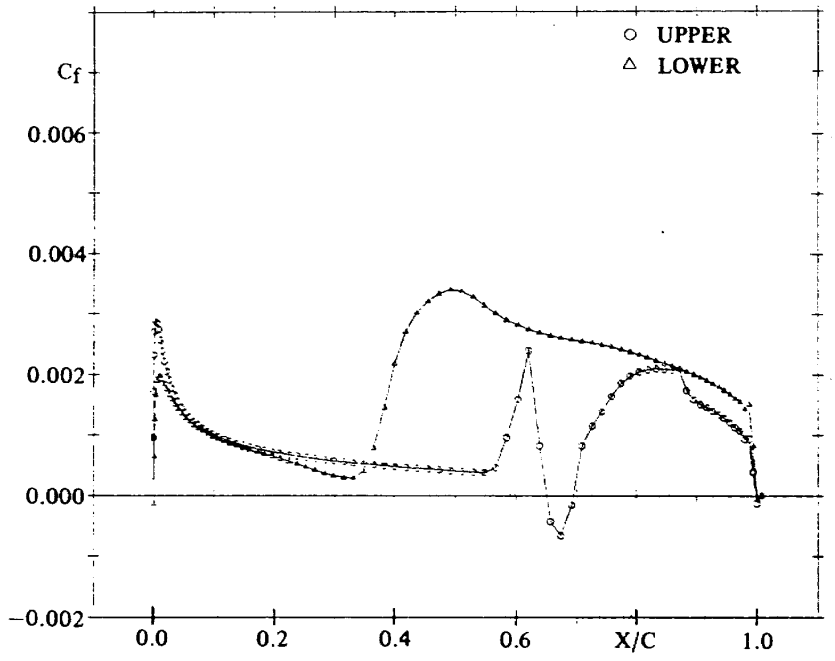

(b) Skin friction coefficient distribution.

Fig. 7 Result for NACA 0012, $M_\infty = 0.8$, $\alpha = 2^\circ$, $Re = 2 \times 10^7$.
Present artificial dissipation. Michel's criterion of transition.
$\kappa_2 = 0.25$, $\kappa_4 = 0.01$, $\epsilon_e = 2.0$, $\epsilon_i = 4.0$,
$C_L = 0.45469$, $C_D = 0.03647$, $C_M = -0.04799$.

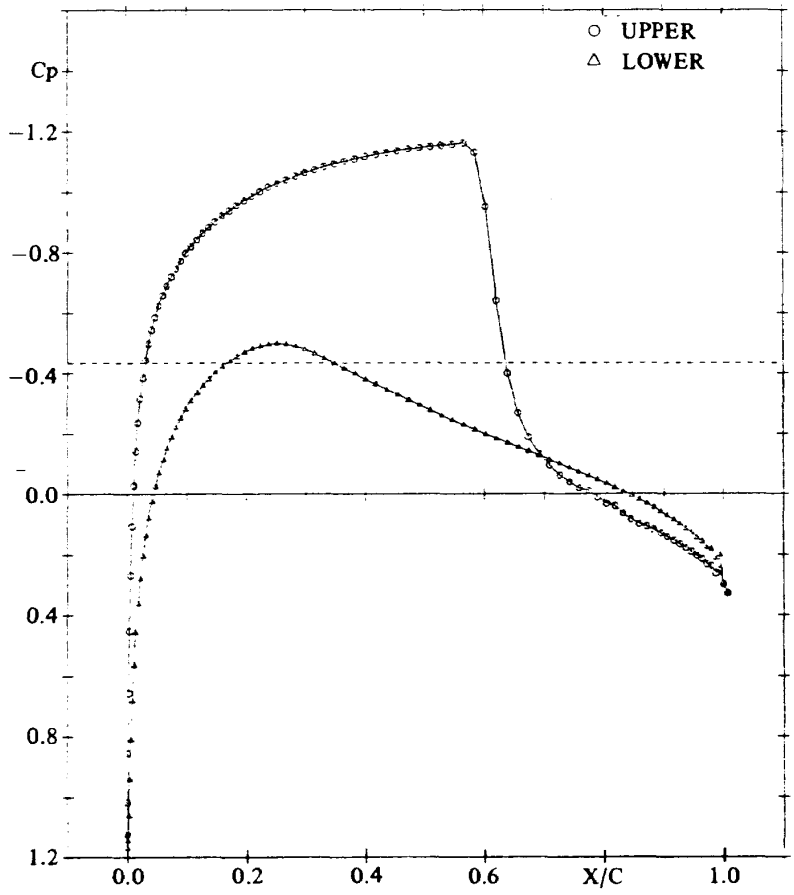

(a) Pressure coefficient distribution.

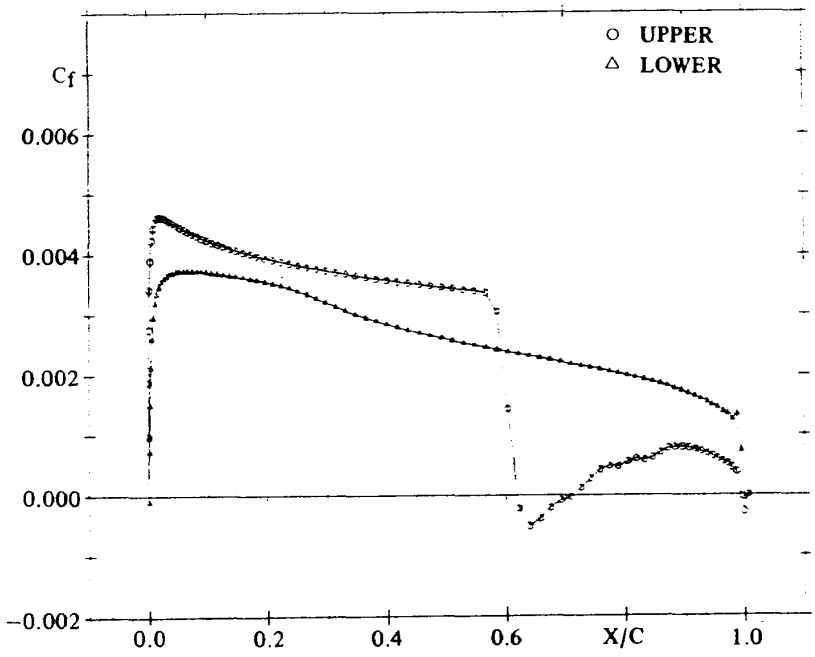

(b) Skin friction coefficient distribution.

Fig. 8 Result for NACA 0012, $M_\infty = 0.8$, $\alpha = 2^\circ$, $Re = 2 \times 10^7$.
Present artificial dissipation. Fully turbulent.
$\kappa_2 = 0.25$, $\kappa_4 = 0.01$, $\epsilon_e = 2.0$, $\epsilon_i = 4.0$,
$C_L = 0.39996$, $C_D = 0.03660$, $C_M = -0.03245$.

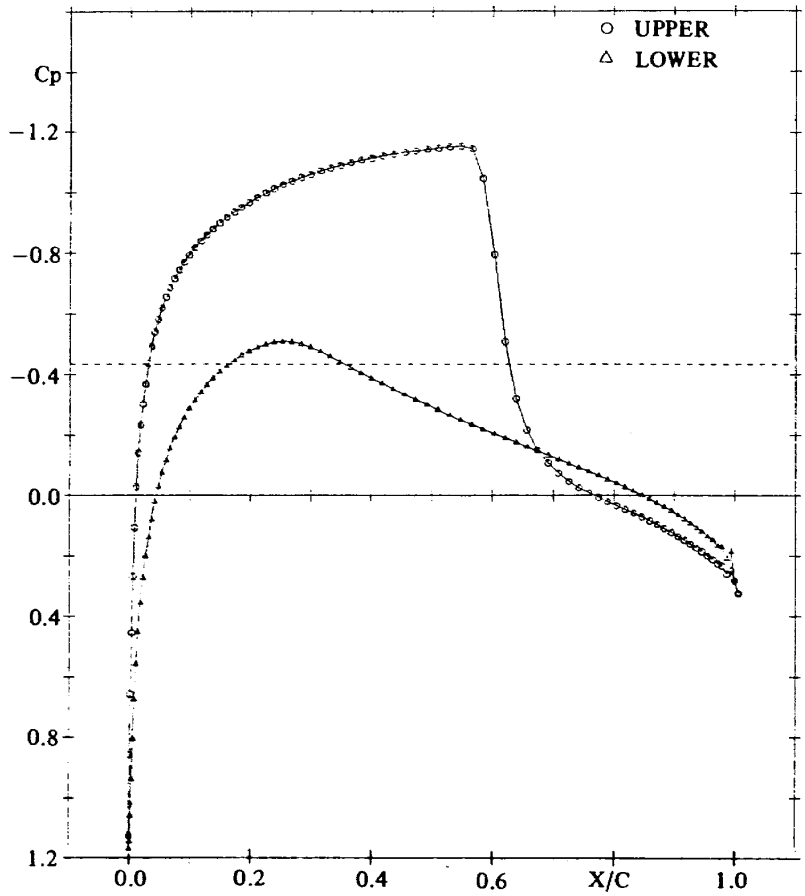

(a) Pressure coefficient distribution.

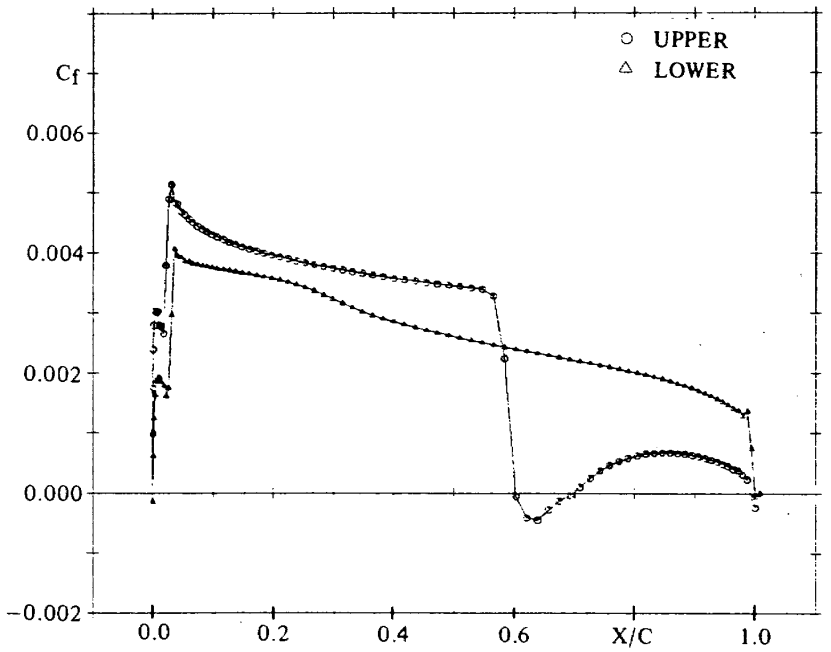

(b) Skin friction coefficient distribution.

Fig. 9 Result for NACA 0012, $M_\infty = 0.8$, $\alpha = 2^\circ$, $Re = 2 \times 10^7$.
Present artificial dissipation. Baldwin-Lomax's criterion of transition.
$\kappa_2 = 0.40$, $\kappa_4 = 0.016$, $\epsilon_e = 2.0$, $\epsilon_i = 4.0$,
$C_L = 0.38029$, $C_D = 0.03533$, $C_M = -0.02679$.

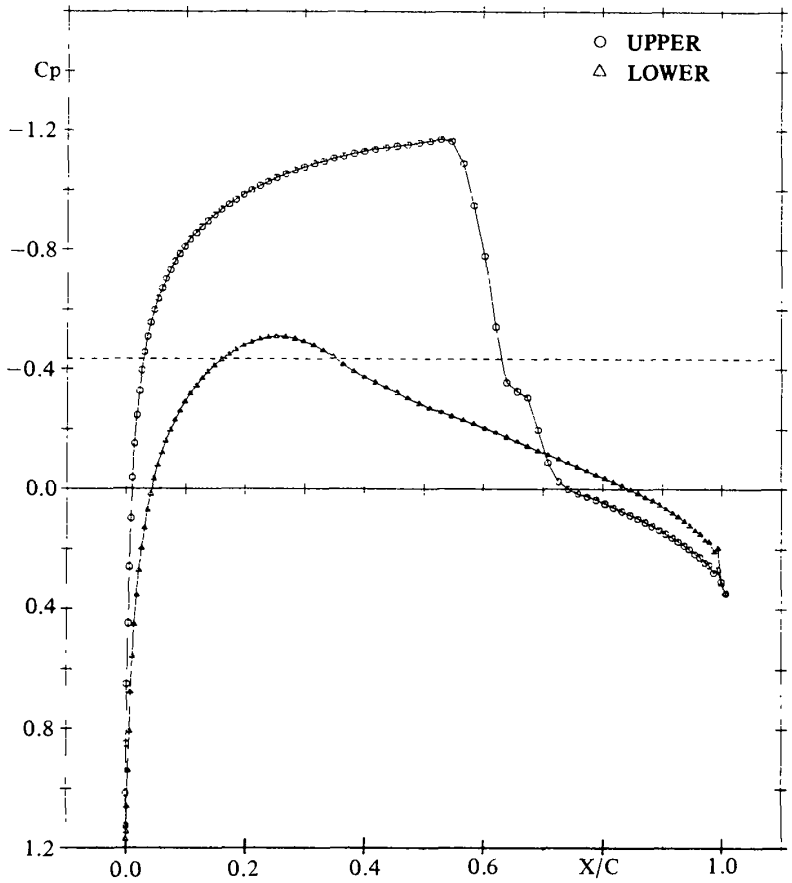

(a) Pressure coefficient distribution.

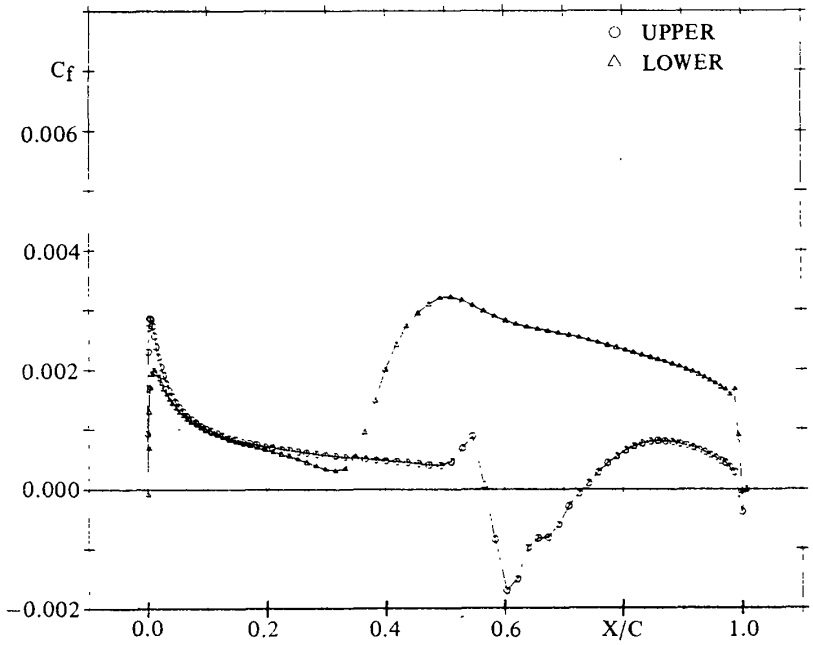

(b) Skin friction coefficient distribution.

Fig. 10 Result for NACA 0012, $M_\infty = 0.8$, $\alpha = 2^\circ$, $Re = 2 \times 10^7$.
Steger's artificial dissipation. Michel's criterion of transition.
$\epsilon_e = 4.0$, $\epsilon_i = 8.0$,
$C_L = 0.39235$, $C_D = 0.03182$, $C_M = -0.02778$.

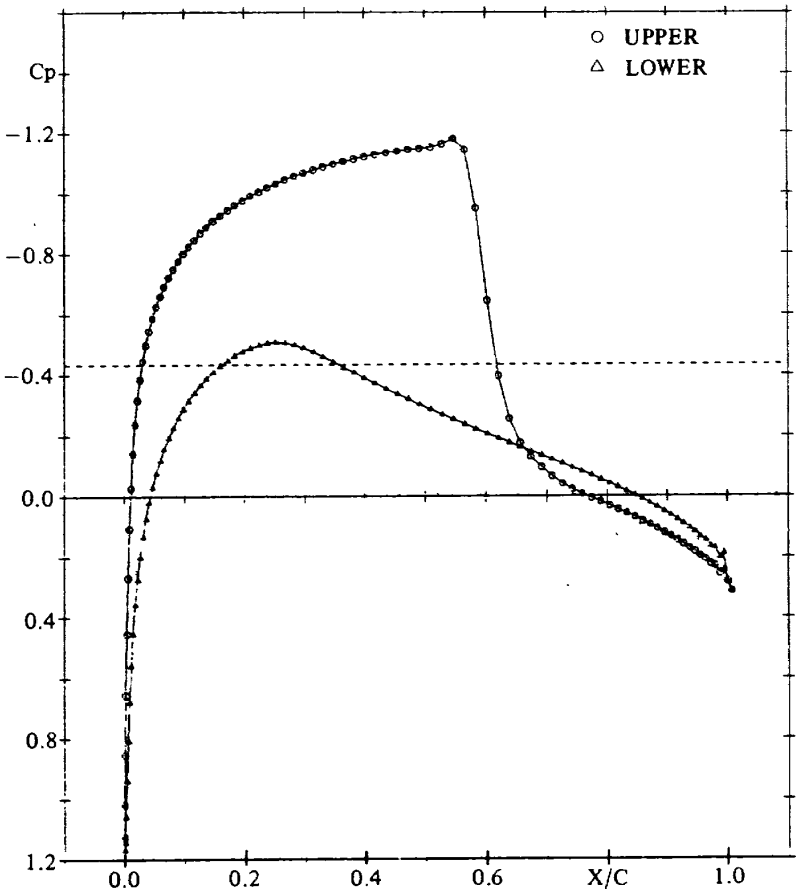

(a) Pressure coefficient distribution.

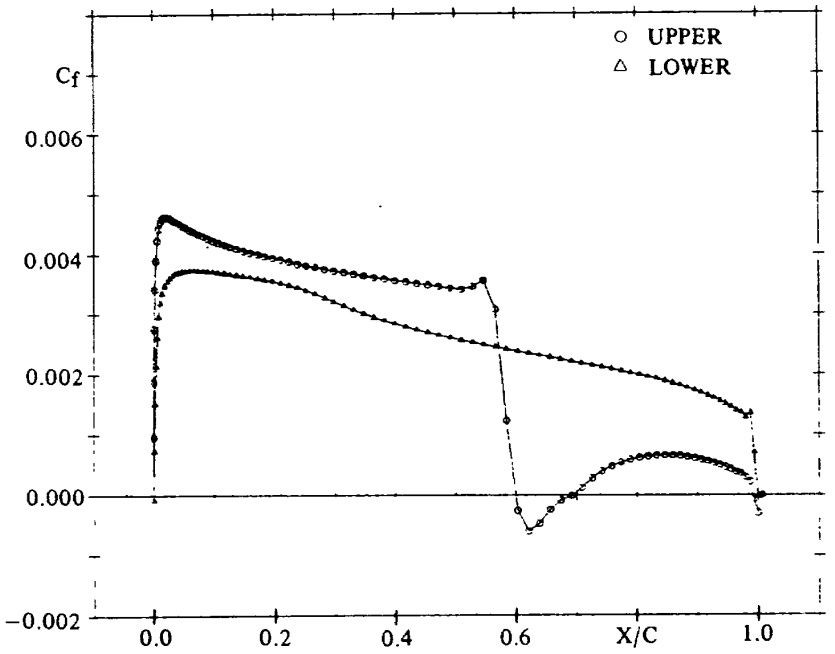

(b) Skin friction coefficient distribution.

Fig. 11 Result for NACA 0012, $M_\infty = 0.8$, $\alpha = 2°$, $Re = 2 \times 10^7$.
Steger's artificial dissipation. Fully turbulent.
$\kappa_e = 4.0$, $\epsilon_i = 8.0$,
$C_L = 0.37445$, $C_D = 0.03424$, $C_M = -0.02347$.

linear artificial dissipation in the η direction, the boundary-layer transition point moves forward due to the spurious viscosity. To avoid this defect of Jameson's type artificial dissipation, we employ Steger's artificial dissipation in the η direction.

7. RESULT FOR GARABEDIAN-KORN 75-06-12 AIRFOIL

To show that the present method for the artificial dissipation can be applied to so called "shockless airfoil", the computation was done for the transonic flow around Garabedian-Korn 75-06-12 airfoil. The flow condition is chosen as; a free stream Mach number of 0.75, attack angles of 0.5, 0.6, 0.7 and 0.8 degree, and a Reynolds number of 20 million. The parameter of boundary-layer transition is chosen as Michel's criterion. The parameters for grid generation are the same as NACA 0012 airfoil case. The grid is composed of 241 points in the ξ direction and 65 points in the η direction. The minimum grid space in the η direction is 1.0×10^{-5}.

Figures 12 through 15 show the pressure coefficient distributions computed under the above conditions. Figure 12 is the result computed under the condition that the attack angle is 0.5 degree, and the computed lift coefficient is 0.550. Figure 13 is the result computed under the condition that the attack angle is 0.6 degree, and the computed lift coefficient is 0.573. Figure 14 is the result computed under the con-

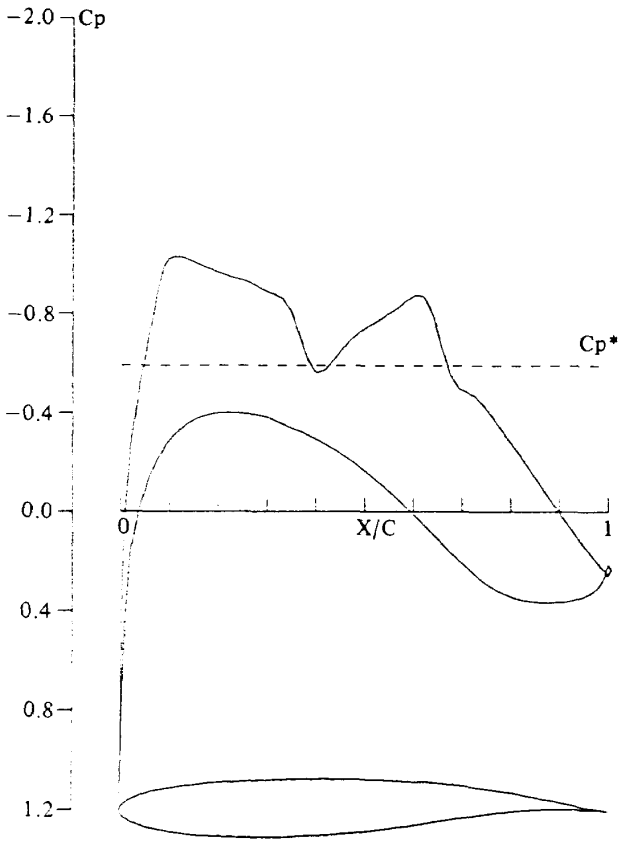

Fig. 12 Pressure coefficient distribution for Garabedian-Korn 75-06-12, M_∞ = 0.75, $\alpha = 0.5^\circ$, $Re = 2 \times 10^7$. Present artificial dissipation, Michel's criterion of transition.
$\kappa_2 = 0.25$, $\kappa_4 = 0.01$, $\epsilon_e = 2.0$, $\epsilon_i = 4.0$,
$C_L = 0.54992$, $C_D = 0.00885$,
$C_M = -0.12723$.

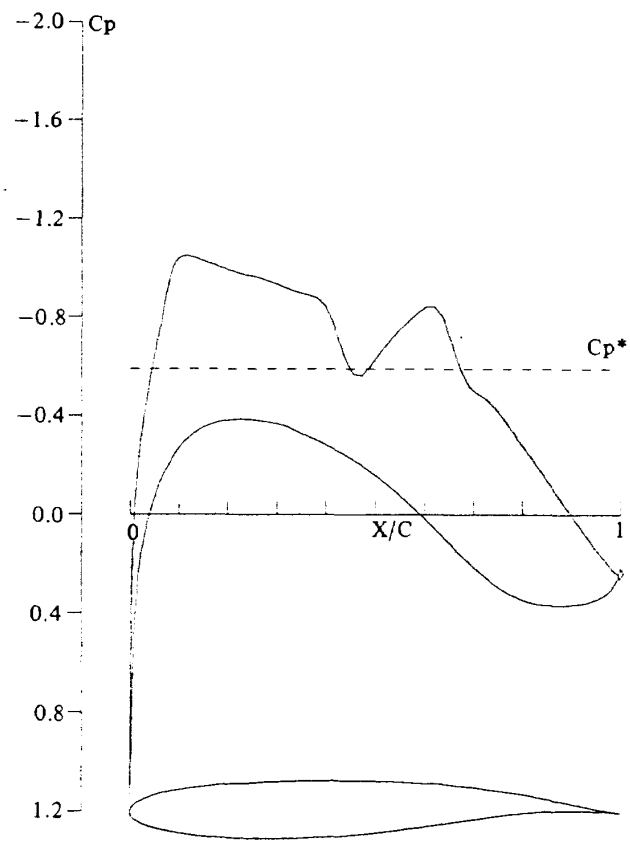

Fig. 13 Pressure coefficient distribution for Garabedian-Korn 75-06-12, M_∞ = 0.75, $\alpha = 0.6^\circ$, $Re = 2 \times 10^7$. Present artificial dissipation, Michel's criterion of transition.
$\kappa_2 = 0.25$, $\kappa_4 = 0.01$, $\epsilon_e = 2.0$, $\epsilon_i = 4.0$,
$C_L = 0.57306$, $C_D = 0.00880$,
$C_M = -0.12678$.

dition that the attack angle is 0.7 degree, and the computed lift coefficient is 0.569. Figure 15 is the result computed under the condition that the attack angle is 0.8 degree, and the computed lift coefficient is 0.621.

None of these distributions of the pressure coefficient achieves a shockless super-critical flow, although the computed lift coefficients are near the design lift coefficient, 0.6. But this fact does not mean the defect of Jameson's type nonlinear artificial dissipation, because the results which are computed using Steger's artificial dissipation are almost the same as the results shown by Figs. 12 through 15. When we restrict grid points in a way 131 points in the ξ direction and 45 points in the η direction, the computed distribution of the pressure coefficient looks like shockless. This is because the numerical solution was smeared around the shock wave by the large truncation error due to coarse grid. We should note that less-smeared numerical solution rarely gives shockless super-critical flow for an airfoil which is designed as shockless using hodograph method but often gives two shock waves as seen in Figs. 12, 13, 14 and 15. This situation is not only true for numerical solutions of the Navier-Stokes equations but also true for numerical solutions of the potential equation.

The results of the present Chapter verify that the present method for the artificial dissipation can be applied to the transonic flow with small shock waves.

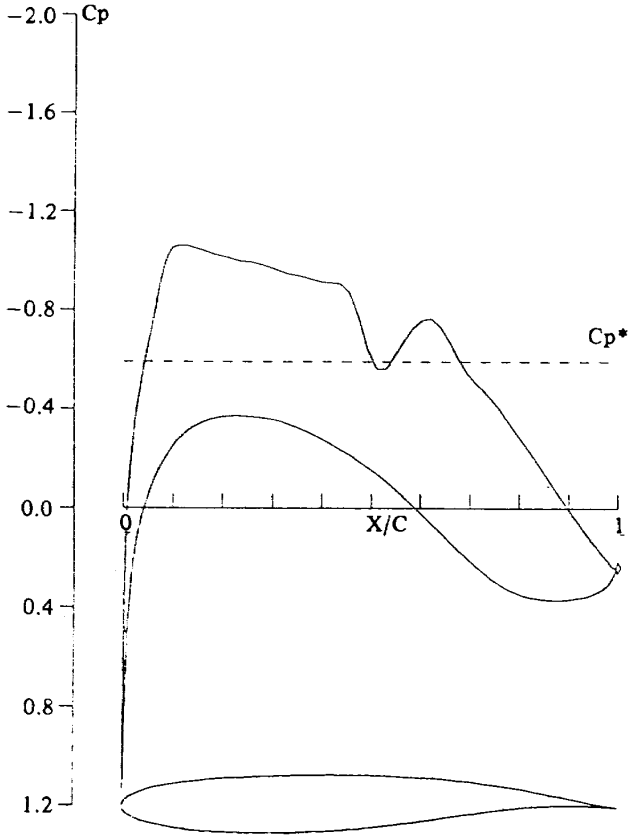

Fig. 14 Pressure coefficient distribution for Garabedian-Korn 75-06-12, M_∞ = 0.75, $\alpha = 0.7°$, $Re = 2 \times 10^7$. Present artificial dissipation, Michel's criterion of transition.
$\kappa_2 = 0.25$, $\kappa_4 = 0.01$, $\epsilon_e = 2.0$, $\epsilon_i = 4.0$,
$C_L = 0.59624$, $C_D = 0.00897$,
$C_M = -0.12652$.

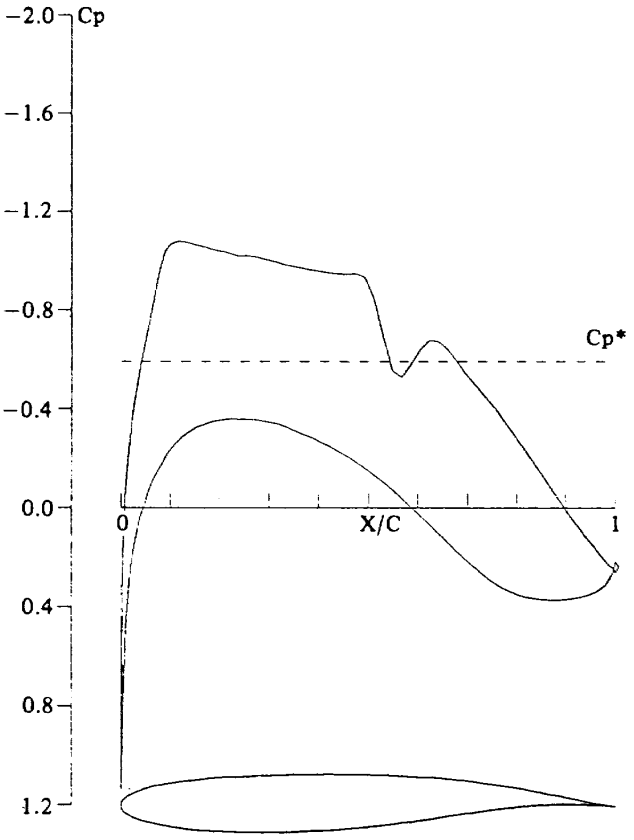

Fig. 15 Pressure coefficient distribution for Garabedian-Korn 75-06-12, M_∞ = 0.75, $\alpha = 0.8°$, $Re = 2 \times 10^7$. Present artificial dissipation, Michel's criterion of transition.
$\kappa_2 = 0.25$, $\kappa_4 = 0.01$, $\epsilon_e = 2.0$, $\epsilon_i = 4.0$,
$C_L = 0.62082$, $C_D = 0.00986$,
$C_M = -0.12704$.

8. RESULT FOR NACA 64_2-015 AIRFOIL

In the present Chapter, we compare the computational results with the experimental data. Abbott and Doenhoff[7] give the drag polar curves of NACA 64_2-015 airfoil at low speed. So, we compute the aerodynamic characteristics of NACA 64_2-015 airfoil at low Mach number.

Since the computational time becomes very large with the Navier-Stokes computation as the Mach number becomes small, we choose the Mach number as 0.2. We choose the Reynolds number as 6 million and the attack angle as 0.0 through 6.8 degree. We do not need negative values of the attack angle, since the airfoil is symmetric. As described at the Appendix D, taking account of the leading edge radius, we increase the points which depict the shape of the airfoil near the leading edge and then we generate a grid around the airfoil. The grid is composed of 241 points in the ξ direction and 65 points in the η direction. The minimum grid space in the η direction is 1.6×10^{-5}, which is larger than that of the previous airfoils because the present value of Reynolds number is smaller than that of the previous cases. 20 points in the η direction near the airfoil is generated algebraically so that the grid near the airfoil be exactly orthogonal to the surface of the airfoil. This orthogonality improves the accuracy of computation especially when we use Michel's criterion of boundary-layer transition. It is because Michel's criterion requires the momentum thickness, which is originally defined along the line normal to an airfoil surface.

Figure 16 shows the drag polar of NACA 64_2-015 airfoil. The solid line indicates the experimental data described by Abbott and Doenhoff[7], the symbols Δ and X indicate the results computed using Baldwin-Lomax's criterion[4] of boundary-layer transition, and the symbols O and + indicate the results computed using Michel's criterion[5] of boundary-layer transition. Moreover, the symbols Δ and O

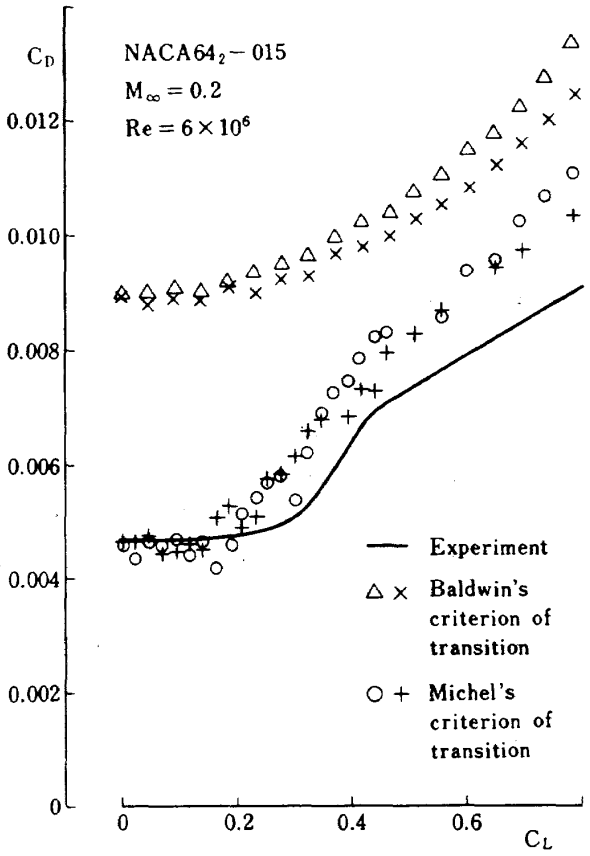

Fig. 16 Computational and experimental drag polar of NACA 64_2-015, $M_\infty = 0.2$, $Re = 6 \times 10^6$.

indicate the results computed using Jameson's type nonlinear artificial dissipation, and X and + indicate the results computed using Steger's artificial dissipation. Comparing computational results with experimental data, we find that Michel's criterion is much better than Baldwin-Lomax's criterion and that the results computed using Michel's criterion are very close to the experimental data in the range where the lift coefficient is small.

We should note that the results computed using Jameson's type artificial dissipation become worse than the results computed using Steger's artificial dissipation as the attack angle or the lift coefficient increases. The notable difference of Jameson's artificial dissipation from Steger's one is the second-order artificial dissipation, and it behaves like a viscous term. From Eqs. (48), (49) and (52), we find that the co-

efficient of the second-difference artificial dissipation becomes large as the second derivative of the pressure becomes large. That is, the spurious viscosity produced by Jameson's type artificial dissipation in the ξ direction becomes noticeably large when the second derivative of the pressure and the computed drag coefficient becomes larger than the ordinary result. Although the second-difference artificial dissipation works well to capture shock wave, it becomes detrimental for subcritical flow if there is large absolute value of the second derivative of the pressure.

Figure 17 shows the distribution of the pressure coefficient computed using Jameson's type nonlinear artificial dissipation. The attack angle is 0.8 degree and the computed lift coefficient is 0.0947. This distribution is so smooth that the absolute value of the second derivative of the pressure is small. Therefore, the detrimental effect of the second-difference artificial dissipation is negligibly small, and the resulting drag coefficient is accurate enough as shown in Fig. 16 (at $C_L \fallingdotseq 0.1$).

Figure 18 shows the distribution of the pressure coefficient computed using Jameson's type nonlinear artificial dissipation. The attack angle is 3.4 degree and the computed lift coefficient is 0.394. This distribution has a peak of the pressure coefficient distribution on the upper surface, and so the absolute value of the second derivative of the pressure is very large at the peak. Therefore, the detrimental effect of the

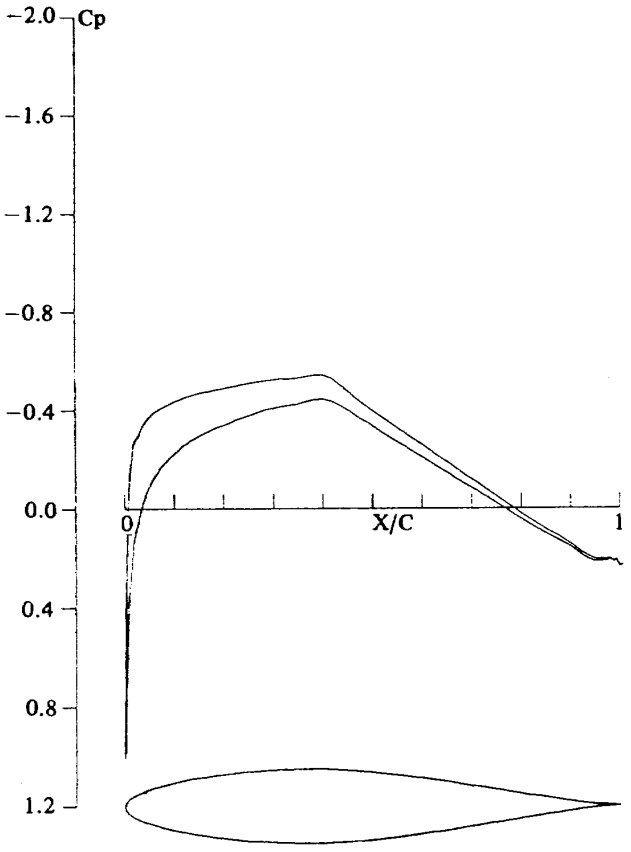

Fig. 17 Pressure coefficient distribution for NACA 64_2-015, $M_\infty = 0.2$, $\alpha = 0.8^\circ$, $Re = 6 \times 10^6$. Present artificial dissipation. Michel's criterion of transition.
$\kappa_2 = 0.25$, $\kappa_4 = 0.01$, $\epsilon_e = 2.0$, $\epsilon_i = 4.0$,
$C_L = 0.09471$, $C_D = 0.00463$,
$C_M = -0.00141$.

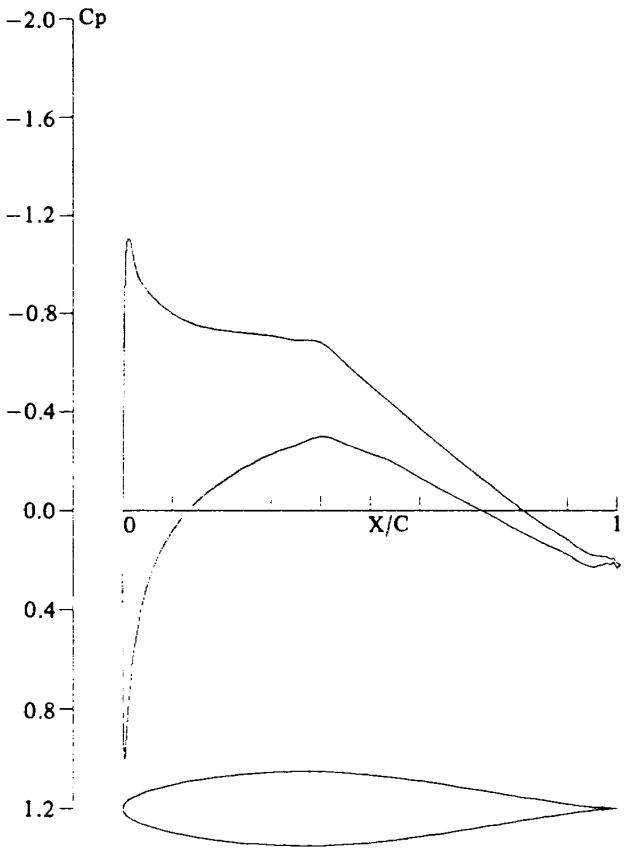

Fig. 18 Pressure coefficient distribution for NACA 64_2-015, $M_\infty = 0.2$, $\alpha = 3.4^\circ$, $Re = 6 \times 10^6$. Present artificial dissipation. Michel's criterion of transition.
$\kappa_2 = 0.25$, $\kappa_4 = 0.01$, $\epsilon_e = 2.0$, $\epsilon_i = 4.0$,
$C_L = 0.39405$, $C_D = 0.00745$,
$C_M = -0.00589$.

second-difference artificial dissipation is very large, and the resulting drag coefficient is worse than the drag coefficient computed using Steger's artificial dissipation as shown in Fig. 16 (at $C_L \fallingdotseq 0.4$).

Now we have found that Jameson's type nonlinear artificial dissipation produces spurious viscosity and that it becomes spurious increase of the drag coefficient. This defect becomes noticeable as the peak of the pressure coefficient distribution grows.

This defect of Jameson's type artificial dissipation is not fatal. One of the recipes for overcoming this defect is to reduce the constant coefficient of the second-difference term of this dissipation, κ_2, to small value (for example, $\kappa_2 = 0.05$) or zero when we compute low-speed flow. In the present report, we retain Steger's artificial dissipation in the two-dimensional Navier-Stokes code, and we choose the appropriate one from Jameson's type and Steger's artificial dissipations.

9. CONCLUSION

Stability analysis of Jameson's type nonlinear artificial dissipation is studied so that this artificial dissipation can be applied to the two-dimensional Navier-Stokes equations within the framework where the resulting system of equations to be solved is block tridiagonal equations. And we have obtained the following conclusions.

(1) The von Neumann stability analysis is made for the model equation. The stability constraint is obtained between the coefficients of the artificial dissipation terms of the model equation. (See Eqs. (25) and (26).)

(2) This stability constraint is applied to Jameson's type nonlinear artificial dissipation terms of the Navier-Stokes equations to determine the implicit part of the artificial dissipation. (See Eqs. (46) and (47).) The present method mainly consists of this determination of the implicit part of Jameson's type nonlinear artificial dissipation, and it is the focus of the present report.

(3) The boundary approximation of the fourth-difference artificial dissipation is shown (See Eqs. (63), (64), (65) and (66).), and its stability analysis is shown.

(4) The results of the practical computation for the flow around an airfoil verify the present method of stability constraint and the boundary approximation.

(5) From the evaluation of the computational results, we find that Jameson's type nonlinear artificial dissipation has a quantitative defect: This dissipation produces spurious viscosity. To avoid this defect, we employ Steger's artificial dissipation in the η direction. When the angle of attack is high, the computed drag coefficient is overestimated for low-speed flow. Therefore we do not employ Jameson's nonlinear artificial dissipation in either ξ or η direction for low-speed flow.

If we pay attention to (5), the present method is a convenient and powerful tool for the Navier-Stokes computation, and is widely useful.

REFERENCES

1) Beam, R. & Warming, R.F., "An Implicit Finite-Difference Algorithm for Hyperbolic Systems in Conservation-Law-Form," J. Comp. Phys., Vol. 22, No. 1, (Sep. 1976), pp. 87-110.

2) Steger, J.L., "Implicit Finite-Difference Simulation of Flow about Arbitrary Two-Dimensional Geometries," AIAA J. Vol. 16, No. 7, (July 1978), pp. 679-686.

3) Pulliam, T.H., "Artificial Dissipation Models for the Euler Equations," AIAA J., Vol. 24, No. 12, (Dec. 1986), pp. 1931-1940 (also appears as AIAA Paper 85-0438 (Jan. 1985)).

4) Baldwin, B. & Lomax, H., "Thin-Layer Approximation and Algebraic Model for Separated Turbulent Flows," AIAA Paper 78-257, (Jan. 1978).

5) Cebeci, T. & Smith, A.M.O., "Analysis of Turbulent Boundary Layers," Chapter 6 (6.2.7), Academic Press, (1974).
6) Richtmyer, R.D. & Morton, K.W., "Difference Method for Initial-Value Problems," Chapter 5 (5.1), Interscience Publishers, second edition, (1967).
7) Abbott, I.H. & von Doenhoff, A.E., "Theory of Wing Sections," Dover Publications, Inc., (1959).
8) Steger, J.L. & Warming, R.F., "Flux Vector Splitting of the Inviscid Gasdynamic Equations With Application to Finite Difference Methods," NASA Technical Memorandum 78605, (July 1979).

APPENDIX A

Supplementary Description of Von Neumann Stability Analysis

In the present Appendix, we describe the detail derivation of Eq. (8) from Eq. (6), following the method of von Neumann stability analysis, and we describe the validity of Eq. (10) in detail.

We write Eq. (6) again as

$$(1 + \lambda\,\delta - a\nabla\Delta)\,(u_j^{n+1} - u_j^n)$$
$$= -\lambda\,\delta\,u_j^n + b\,\nabla\Delta\,u_j^n - \beta_4\,(\nabla\Delta)^2\,u_j^n \qquad \text{(A1)}$$

and rewrite the definition (7) as

$$u_j^{n+1} = g\,u_j^n \qquad \text{(A2)}$$

First we put

$$u_j^n = v^n\,e^{i\omega j} \qquad \text{(A3)}$$

where ω = (wave number) $\times$ (Δx) and i is the imaginary unit. Equation (A3) implies that u is expressed by a Fourier component. By Eq. (A3), the movement of index is reduced to the factorization of exponent as described by the following formula.

$$u_{j+m} = v\,e^{i\omega(j+m)} = e^{im\omega}\,v\,e^{i\omega j}$$
$$= e^{im\omega}\,u_j \qquad \text{(A4)}$$

Equation (A4) is valid for any real value of m, but usually m takes integer value. Applying Eq. (A4), central difference is expressed as

$$\delta\,u_j = (u_{j+1} - u_{j-1})/2$$
$$= \frac{e^{i\omega} - e^{-i\omega}}{2}\,u_j = u_j\,i\sin\omega \qquad \text{(A5)}$$

Similarly, second derivative is expressed as

$$\nabla\Delta\,u_j = u_{j+1} - 2\,u_j + u_{j-1}$$
$$= (e^{i\omega} - 2 + e^{-i\omega})\,u_j$$
$$= (2\cos\omega - 2)\,u_j \qquad \text{(A6)}$$

Fourth derivative is expressed as

$$(\nabla\Delta)^2 u_j = u_{j+2} - 4u_{j+1} + 6\,u_j - 4\,u_{j-1} + u_{j-2}$$

$$= (e^{2i\omega} - 4e^{i\omega} + 6 - 4e^{-i\omega} + e^{-2i\omega})\, u_j$$

$$= (2\cos 2\omega - 8\cos\omega + 6)\, u_j$$

$$= (2(2\cos^2\omega - 1) - 8\cos\omega + 6)\, u_j$$

$$= (2\cos\omega - 2)^2\, u_j \qquad \text{(A7)}$$

Substituting Eqs. (A2), (A5), (A6) and (A7) into Eq. (A1), we get

$$[1 + i\lambda\sin\omega - a(2\cos\omega - 2)]\,(g-1)\,u_j^n$$
$$= -(i\lambda\sin\omega)\,u_j^n + b(2\cos\omega - 2)\,u_j^n$$
$$- \beta_4 (2\cos\omega - 2)^2\, u_j^n \qquad \text{(A8)}$$

Rearranging Eq. (A8), we get

$$g\,[1 + i\lambda\sin\omega - a(2\cos\omega - 2)]$$
$$= 1 + (b-a)(2\cos\omega - 2)$$
$$- \beta_4\,(2\cos\omega - 2)^2 \qquad \text{(A9)}$$

Rearranging Eq. (A9), we get the following equation.

$$g = \frac{1 + 2(a-b)(1-\cos\omega) - 4\beta_4\,(1-\cos\omega)^2}{1 + 2a(1-\cos\omega) + i\lambda\sin\omega} \qquad \text{(A10)}$$

Equation (A10) is exactly Eq. (8). That means that the derivation of Eq. (8) has been completed.

Denoting the numerator of Eq. (A10) as A, and the real part of the denominator as B, we can rewrite Eq. (A10) as

$$g = \frac{A}{B + i\lambda\sin\omega} \qquad \text{(A11)}$$

If we exclude the convection term from Eq. (A11) by puting

$$\lambda\sin\omega = 0 \qquad \text{(A12)}$$

then Equation (A11) changes to

$$g_0 = \frac{A}{B} \qquad \text{(A13)}$$

To compare the magnitude of g and g_0, we compute the absolute values of Eqs. (A11) and (A13), noting that A and B real by definition.

$$|g| = \sqrt{\frac{A^2}{B^2 + \lambda^2\sin^2\omega}} \qquad \text{(A14)}$$

$$|g_0| = \frac{|A|}{|B|} \qquad \text{(A15)}$$

Comparing Eqs. (A14) and (A15), we find

$$|g| \leqq |g_0| \qquad \text{(A16)}$$

Therefore, if g_0 satisfy the stability bound

$$|g_0| \leqq 1 \qquad \text{(A17)}$$

then g satisfies the stability bound

$$|g| \leqq 1 \qquad \text{(A18)}$$

as well. That means that we only have to examine the von Neumann stability constraint for Eq. (A13). If we rename g_0 to g, Equation (A13) becomes Eq. (10).

APPENDIX B

Equivalence of Upwind Difference to Central Difference Plus Artificial Dissipation

In the present Appendix, we show that the first-order-accurate upwind difference is equivalent to second-order-accurate central difference plus second-differnce artificial dissipation.

As an example of first-order-accurate upwind difference, we take backward difference and analyze it as follows.

$$\nabla_\xi \hat{E}_j = \hat{E}_j - \hat{E}_{j-1} = \frac{1}{2}(\hat{E}_{j+1} - \hat{E}_{j-1})$$
$$- \frac{1}{2}(\hat{E}_{j+1} - 2\hat{E}_j + \hat{E}_{j-1}) \qquad \text{(B1)}$$

By the definition of the difference operators, Equation (B1) becomes

$$\nabla_\xi \hat{E}_j = \delta_\xi \hat{E}_j - \frac{1}{2}\nabla_\xi \Delta_\xi \hat{E}_j \qquad \text{(B2)}$$

If $\hat{E}$ is the flux vector of the Navier-Stokes equations, the following equation is valid[8].

$$\hat{E} = \hat{A}\,\hat{Q} \qquad \text{(B3)}$$

where

$$\hat{A} = \partial\hat{E}/\partial\hat{Q} \qquad \text{(B4)}$$

Substituting Eq. (B3) into Eq. (B2), we get

$$\nabla_\xi \hat{E}_j = \delta_\xi \hat{E}_j - \frac{1}{2}\nabla_\xi \Delta_\xi \hat{A}_j\,\hat{Q}_j \qquad \text{(B5)}$$

We can replace $\hat{A}$ by its spectral radius σ, which is a typical norm of matrix, in approximate sense. Then Equation (B5) can be approximated

by

$$\nabla_\xi \hat{E}_j = \delta_\xi \hat{E}_j - \frac{1}{2}\nabla_\xi \Delta_\xi \sigma_j \hat{Q}_j \qquad \text{(B6)}$$

The last term of Eq. (B6) is second-difference artificial dissipation. Equation (B6) shows that first-order-accurate upwind difference is equivalent to second-order-accurate central difference plus second-difference artificial dissipation.

We should note that the right-hand side of Eq. (B6) is more flexible than the left-hand side. It is because we can modify the coefficient of the artificial dissipation term, $\frac{1}{2}$, to other constant or variable, and because we can modify the form of the artificial dissipation. One of modifications is described as follows.

$$\frac{1}{2}\nabla_\xi \Delta_\xi \sigma_j \hat{Q}_j$$

$$\sim \frac{1}{2}\nabla_\xi (\sigma J^{-1})_{j+\frac{1}{2}} \Delta_\xi J_j \hat{Q}_j$$

$$\fallingdotseq \frac{1}{4}\nabla_\xi (\sigma_{j+1} J_{j+1}^{-1} + \sigma_j J_j^{-1}) \Delta_\xi J_j \hat{Q}_j \qquad \text{(B7)}$$

The right-hand side of Eq. (B7) is the basic form of the second-difference part of Jameson's type artificial dissipation.

Although the left-hand side of IAF scheme is complex, its essential feature can be described by

$$\partial_\xi \hat{A}\ \delta\ \hat{Q} \qquad \text{(B8)}$$

for the convection term in the ξ direction. Therefore, all the relations corresponding to the above equations can be deduced by replacing $\hat{E}$ by $\hat{A}\,\delta\,\hat{Q}$. From Eq. (B2), we get

$$\nabla_\xi \hat{A}_j \delta \hat{Q}_j = \delta_\xi \hat{A}_j \delta \hat{Q}_j - \frac{1}{2}\nabla_\xi \Delta_\xi \hat{A}_j\ \delta\ \hat{Q}_j \qquad \text{(B9)}$$

Replacing $\hat{A}$ by its spectral radius σ, we get the following approximation.

$$\nabla_\xi \hat{A}_j\ \delta \hat{Q}_j = \delta_\xi \hat{A}_j\ \delta\ \hat{Q}_j - \frac{1}{2}\nabla_\xi \Delta_\xi \sigma_j\ \delta\ \hat{Q}_j \qquad \text{(B10)}$$

The last term of Eq. (B10) is exactly the same as the last term of Eq. (B6) and is second-difference artificial dissipation. Therefore its modification is described by Eq. (B7).

By Eqs. (B6), (B10) and (B7), we find that we should use central difference for the convection terms, $\partial_\xi \hat{A}\,\delta\,\hat{Q}$ and $\partial_\xi \hat{E}$, of the Navier-Stokes equations in IAF scheme when we employ Jameson's type artificial dissipation.

General discussion on the equivalence of upwind difference to central difference plus artificial dissipation is described in Reference 3.

APPENDIX C

Particular Solution of $du/dt = Au$

In the present Appendix, we will show the well-known solution of the following vector-matrix equation.

$$\frac{d}{dt}\boldsymbol{u} = \boldsymbol{A}\,\boldsymbol{u} \qquad \text{(C1)}$$

Here $\boldsymbol{u}$ is a m-component column vector, $\boldsymbol{A}$ is a $m \times m$ matrix, and t is a scalar.

Since $\exp(\boldsymbol{A}t)$ is defined by the sum of the infinite series of $(\boldsymbol{A}t)^n/n!$ $(n = 0, 1, 3, \ldots)$, the following analysis is valid.

$$\begin{aligned} & d/dt\ [\exp(\boldsymbol{A}t)] \\ &= d/dt\ [I + \boldsymbol{A}t + (\boldsymbol{A}t)^2/2! + (\boldsymbol{A}t)^3/3! + \ldots.] \\ &= \quad 0 + \boldsymbol{A} + \boldsymbol{A}^2 t \quad + \boldsymbol{A}^3 t^2/2! + \ldots. \\ &= \boldsymbol{A}\ [I + \boldsymbol{A}t + \boldsymbol{A}^2 t^2/2! + \boldsymbol{A}^3 t^3/3! + \ldots.] \\ &= \boldsymbol{A}\ \exp(\boldsymbol{A}t) \end{aligned} \qquad \text{(C2)}$$

From Eq. (C2), we find

$$\boldsymbol{u} = \exp(\boldsymbol{A}t) \qquad \text{(C3)}$$

is a particular solution of Eq. (C1).

It is difficult to find the property of the solution if the formula of the solution is written by Eq. (C3). So, we assume that we are able to diagonalize the matrix $\boldsymbol{A}$ as

$$\boldsymbol{S}^{-1}\boldsymbol{A}\,\boldsymbol{S} = \Lambda \qquad \text{(C4)}$$

Here Λ is a diagonal matrix and its diagonal components, $\lambda_1, \lambda_2, \lambda_3, \ldots, \lambda_m$, are the eigenvalues of $\boldsymbol{A}$. Using Eq. (C4), we can get the following formula.

$$
\begin{aligned}
&\exp(At) \\
&= I + S\Lambda S^{-1} t + S\Lambda S^{-1} S\Lambda S^{-1} t^2/2! \\
&\quad + S\Lambda S^{-1} S\Lambda S^{-1} S\Lambda S^{-1} t/3! + \ldots \\
&= I + S\Lambda S^{-1} t + S\Lambda^2 S^{-1} t^2/2! \\
&\qquad + S\Lambda^3 S^{-1} t^3/3! + \ldots \\
&= S\ [I + \Lambda t + (\Lambda t)^2/2! + (\Lambda t)^3/3! + \ldots]\ S^{-1} \\
&= S \exp(\Lambda t) S^{-1} \qquad \text{(C5)}
\end{aligned}
$$

To examine what $\exp(\Lambda t)$ is, we use the following formulae.

$$
\Lambda = \begin{bmatrix} \lambda_1 & & O \\ & \lambda_2 & \\ & & \ddots \\ O & & \lambda_m \end{bmatrix}, \Lambda^2 = \begin{bmatrix} \lambda_1^2 & & O \\ & \lambda_2^2 & \\ & & \ddots \\ O & & \lambda_m^2 \end{bmatrix},
$$

$$
\Lambda^3 = \begin{bmatrix} \lambda_1^3 & & O \\ & \lambda_2^3 & \\ & & \ddots \\ O & & \lambda_m^3 \end{bmatrix}, \ldots \qquad \text{(C6)}
$$

Substituting Eq. (C6) into the definition of $\exp(\Lambda t)$, we get

$$
\begin{aligned}
\exp(\Lambda t) &= I + \Lambda t + (\Lambda t)^2/2! + (\Lambda t)^3/3! + \ldots \\
&= \begin{bmatrix} 1 & & O \\ & 1 & \\ & & \ddots \\ O & & 1 \end{bmatrix} + \begin{bmatrix} \lambda_1 & & O \\ & \lambda_2 & \\ & & \ddots \\ O & & \lambda_m \end{bmatrix} t + \\
&\quad \begin{bmatrix} \lambda_2^2 & & O \\ & \lambda_3^2 & \\ & & \ddots \\ O & & \lambda_m^2 \end{bmatrix} \frac{t^2}{2!} + \begin{bmatrix} \lambda_2^3 & & O \\ & \lambda_3^3 & \\ & & \ddots \\ O & & \lambda_m^3 \end{bmatrix} \frac{t^3}{3!} + \ldots \\
&= \begin{bmatrix} \exp(\lambda_1 t) & & O \\ & \exp(\lambda_2 t) & \\ & & \ddots \\ O & & \exp(\lambda_m t) \end{bmatrix} \qquad \text{(C7)}
\end{aligned}
$$

Equation (C7) gives us easy understanding of $\exp(\Lambda t)$, since $\exp(\lambda_1 t)$, $\exp(\lambda_2 t), \ldots,$ $\exp(\lambda_m t)$ are scalar. Substituting Eq. (C7) into Eq. (C5) and substituting the resultant equation into Eq. (C3), we obtain

$$
\boldsymbol{u} = S \begin{bmatrix} \exp(\lambda_1 t) & & O \\ & \exp(\lambda_2 t) & \\ & & \ddots \\ O & & \exp(\lambda_m t) \end{bmatrix} S^{-1} \qquad \text{(C8)}
$$

as a particular solution of Eq. (C1).

APPENDIX D

Curve Fitting near the Leading Edge of an Airfoil

Before we generate grid around an airfoil, as input data we require many points which depict the airfoil. Unless we have enough points of an airfoil, we cannot depict the airfoil accurately, and as a result we will get a bad pressure distribution. In the case of an NACA 00XX series airfoil, we can get as many points as we need, since the airfoil is described analytically. But an NACA 6-series airfoil[7] gives us sparse points near the leading edge, while it gives us a leading edge radius. Therefore, to obtain good result for an NACA 6-series airfoil, we have to make use of the information of the leading edge radius. We describe below one of the ways to increase the points which depict approximately the geometry near the leading edge of the airfoil by taking account of the leading edge radius.

Let us approximate the curve near the leading edge of an airfoil by the following fourth-order polynomial.

$$x = -ay^4 + by^2 \tag{D1}$$

Here we have assumed that the airfoil is symmetric with regard to $y = 0$ line and that the leading edge is placed at the origin $(x, y) = (0, 0)$. The derivatives of Eq. (D1) are

$$x' = -4ay^3 + 2by \tag{D2}$$

$$x'' = -12ay^2 + 2b \tag{D3}$$

If r denotes the radius of the leading edge at the point $(x, y) = (0, 0)$, we get

$$\frac{1}{r} = \frac{x''}{[1 + (x')^2]^{3/2}} = 2b$$

$$\therefore b = 1/(2r) \tag{D4}$$

Letting the curve described by Eq. (D1) pass through the specified point $(x, y) = (x_*, y_*)$, we get

$$a = \frac{by_*^2 - x_*}{y_*^4} \tag{D5}$$

Here we have found that the constants, a and b, become known.

If we want y to be a function of x, we apply the formula of the roots of a second-order polynomial equation to Eq. (D1). Then we get

$$y^2 = \frac{b - \sqrt{b^2 - 4ax}}{2a} \tag{D6}$$

Here we have selected the solution which satisfies $(x, y) = (0, 0)$. To improve the numerical accuracy, Equation (D6) is rewritten as

$$y^2 = \frac{2x}{b + \sqrt{b^2 - 4ax}} \tag{D7}$$

Equation (D7) with Eqs. (D4) and (D5) is actually used when we increase 8 points near the leading edge of NACA 64_2-015 airfoil to approximately form the geometry near the leading edge by taking account of the leading edge radius.

TECHNICAL REPORT OF NATIONAL
AEROSPACE LABORATORY
TR-1015T

航空宇宙技術研究所報告1015T号（欧文）

平成元年2月発行

発行所　航空宇宙技術研究所
東京都調布市深大寺東町7丁目44番地1
電話三鷹(0422) 47-5911（大代表）〒182
印刷所　株式会社　東京プレス
東京都板橋区桜川2－27－12

Published by
NATIONAL AEROSPACE LABORATORY
7-44-1 Jindaijihigashi-Machi Chōfu, Tokyo
JAPAN

Printed in Japan